Geochimica et Cosmochimica Acta 404 (2025) 134–149

Contents lists available at ScienceDirect

Geochimica et Cosmochimica Acta

journal homepage: www.elsevier.com/locate/gca

Uranium reduction in modern and ancient marine carbonate settings – insights from anaerobic U extractions and high-energy resolution X ray spectroscopy

Kasper Primdahl Olesen [a], Elvira Bura-Nakic [b], Ivan N. Pidchenko [c], Kristina O. Kvashnina [d,e], Tais W. Dahl [f,g,h,*]

[a] Nordic Center for Earth Evolution, Department of Biology, University of Southern Denmark, Campusvej 55, 5230 Odense M, DK-5230, Denmark
[b] Department for Marine and Environmental Research, "Ruđer Bošković" Institute, Bijenička cesta 54, 10000 Zagreb, Croatia
[c] Department of Biology and Environmental Science, Linnaeus University, SE-39182 Kalmar, Sweden
[d] The Rossendorf Beamline, European Synchrotron Radiation Facility, 71, Avenue des Martyrs, CS 40220, 38043 Grenoble Cedex 9, France
[e] Helmholtz-Zentrum Dresden-Rossendorf, Institute of Resource Ecology, Bautzner Landstraße 400, 01328 Dresden, Germany
[f] Globe Institute, University of Copenhagen, Øster Voldgade 5–7, 1350 Copenhagen, Denmark
[g] State Key Laboratory of Geological Processes and Mineral Resources, China University of Geosciences, Wuhan 430074, China
[h] Department of Geoscience and Natural Resource Management, University of Copenhagen, Øster Voldgade 10, 1350 Copenhagen, Denmark

ARTICLE INFO

Associate Editor: Susan Halsall Little

Keywords:
Uranium oxidation states
Uranium cycling
Marine carbonate sediments
Anaerobic ion chromatography
U isotope fractionation

ABSTRACT

In the marine environment, hexavalent uranium, U^{6+}, is incorporated into primary carbonate minerals with the same isotopic composition ($\delta^{238}U$) as the seawater in which they are formed. Yet, modern marine carbonate sediments carry heavier U isotope compositions. This enrichment of heavy U isotopes has been linked to biogenic U reduction in and below the Fe-reducing zone inside the sediment. Still, the oxidation state(s) of uranium in marine carbonate sediments undergoing syndepositional diagenesis has never been measured before. Here, we 1) present an anaerobic ion chromatographic technique based on the TEVA® resin to chemically separate and quantify abundances of tetravalent U^{4+} and hexavalent U^{6+} fractions in the carbonate, and 2) compare the results from ion chromatography to U L3 edge HERFD-XANES spectroscopic measurements of the total U in sediments to 3) estimate U oxidation states of fresh carbonate sediments from a modern seawater-fed lake and ancient limestones. We find that our anaerobic extraction technique can provide credible evaluations of reduced U^{4+} and oxidized U^{6+} contents, applicable to carbonate sediments and rocks. Our results show that U resides both in reduced and oxidized states in modern carbonate sediments and ancient carbonate rocks. By comparing air-exposed, oven-dried samples to samples always kept under strictly anaerobic condition, we find that the majority of authigenic U in modern carbonate sediments resides in oxidation-sensitive phases that accumulate with sediment depth, instead of being structurally bound in carbonate minerals (aragonite and calcite). We propose a model to account for the observed trends in U oxidation state, U phase associations, and U isotope fractionation, where a substantial fraction of U in the sediments is likely delivered via microbial reduction and precipitated as a non-crystalline, reduced form near the sediment–water interface. We suggest these oxidation-sensitive reduced U species participate in redox cycling where some U is re-oxidized and perhaps bio-reduced again later, for example in the presence of Fe(III) mineral surfaces that undergo reductive dissolution with depth. Simultaneously, a continued incorporation of recalcitrant and isotopically light (i.e. ^{238}U-depleted) U from the pore fluids into diagenetic carbonate may occur. The determination of U oxidation states in modern carbonates in this study helps to bridge a gap in our knowledge of how U isotope signals are affected by *syn*-sedimentary diagenetic U transformations, opening new avenues for understanding sedimentary U cycling and improving the $\delta^{238}U$ paleo redox proxy.

* Corresponding author at: Globe Institute, University of Copenhagen, Øster Voldgade 5–7, 1350 Copenhagen, Denmark.
E-mail address: twd@ign.ku.dk (T.W. Dahl).

https://doi.org/10.1016/j.gca.2025.07.006
Received 11 February 2024; Accepted 4 July 2025
Available online 7 July 2025

1. Introduction

The oxygenation of the atmosphere and oceans, and the evolution of life and the environment have been inseparably linked since the first appearance of appreciable atmospheric O_2 concentrations at the Great Oxidation Event (GOE) ~ 2.3 billion years ago (e.g. Berner et al., 2007; Canfield, 2005; Cole et al., 2020; Holland, 2002; Holland, 2006; Lenton et al., 2014; Lyons et al., 2014; Reinhard et al., 2016). Unraveling these relationships through the reconstruction of Earth's oxygenation and environmental history and understanding the feedback and driving mechanisms in the co-evolution of life and the environment are key goals of modern geochemistry. Ocean oxygenation records are constructed and improved using an increasing range of sedimentological, mineralogical, and geochemical lines of evidence. Variations in the $\delta^{238}U$ value in ancient sediments – defined as the $^{238}U/^{235}U$ part per thousand deviation from the universal reference material CRM-145 – are widely taken to reflect the reduction and immobilization of uranium under anoxic depositional conditions and used to reconstruct ocean oxygenation through Earth's history (e.g., Andersen et al., 2014; Dahl et al., 2014; Zhang et al., 2020).

This palaeoredox application of U isotopes is rooted in the environmental occurrence of U in its reduced and oxidized forms; i.e., U^{4+} and U^{6+}. Here, we adopt the ionic notation, U^{4+} and U^{6+}, rather than U(IV) and U(VI) to ease the reading despite referring only to the electronic charge of the element (i.e., valence state) and not its speciation. Soluble U^{6+} is stable in oxygenated seawater as various Ca/Mg-triscarbonato species of the uranyl UO_2^{2+} ion depending on pH, pCO_2, and cation composition (e.g. Chen et al., 2017; Dong and Brooks, 2006; Langmuir, 1978), and can be reductively immobilized as sparingly soluble U^{4+} species either through biotic pathways (e.g. metal- and sulfate reducing bacteria) or abiotic pathways (e.g. ferrous iron and sulfide) (Wall and Krumholz, 2006). Such U reduction mainly occurs within sediments at or very close to the seawater-sediment interface regardless of water column anoxia, though partial U removal from the water-column is well demonstrated in strongly euxinic systems (Anderson et al., 1989; Chen et al., 2021; Rolison et al., 2017). The biotic reduction products of U present in marine sediments likely consists of mononuclear U^{4+}-phosphate/silicate complexes and to lesser extent nano-crystalline U^{4+}-phosphate of the ningyoite-rhabdophane group, or possibly nano-crystalline and/or crystalline uraninite (UO_2) or other U oxides (Janeczek et al., 1993; Morin et al., 2016; Roebbert et al., 2021; Vettese et al., 2020). Thus, the reduced U phases are likely embedded in an organic matrix in the sediments.

The reduction of U is associated with a considerable enrichment of ^{238}U relative to ^{235}U, presumably arising from stable isotopic fractionation during microbial U reduction (Andersen et al., 2017; Rademacher et al., 2006; Stirling et al., 2007; Stylo et al., 2015; Weyer et al., 2008). Experimentally determined isotope fractionation factors are dependent on U reduction rate and range between $\varepsilon = 0.36$ and $\varepsilon = 0.96$ for microbial reduction and $\varepsilon = 0.23$ and $\varepsilon = 0.83$ for abiotic reduction (Basu et al., 2020; Brown et al., 2018). In the marine realm, anoxic sediments express the largest U isotope fractionation with $\Delta^{238}U_{sediment-}$ offsets of ~ 0.7 ‰ from the global seawater isotopic composition of $\delta^{238}U = -0.39$ ‰ (Andersen et al., 2017; Dahl et al., 2014; Holmden et al., 2015; Noordmann et al., 2015). The main U sinks in the modern ocean are anoxic and suboxic sediments and U is assumed to be well mixed with a residence time of ~ 400 ky (Dunk et al., 2002; Tissot and Dauphas, 2015). Consequently, changes in $\delta^{238}U_{seawater}$ are inferred to reflect changes in the global extent of anoxic seafloor, allowing its use as a quantitative palaeoredox proxy in lithologies where the $\delta^{238}U_{sample}$ reliably identifies coeval $\delta^{238}U_{seawater}$.

Carbonate sedimentary rocks are widely used targets for paleo-seawater $\delta^{238}U$ reconstructions since coprecipitation of U^{6+} with biogenic skeletal carbonate minerals (both aragonite and calcite) preserve the parent $\delta^{238}U$ value in the modern ocean, and because the carbonate rock record provides higher temporal continuity and better spatial connection to the open ocean than other lithologies (Chen et al., 2017; Chen et al., 2016b; Livermore et al., 2020; Morse and Mackenzie, 1990). Some characterization of U in carbonate mineral lattices exists (e.g., Kelly et al., 2007; Kelly et al., 2003; Kelly et al., 2006; Pingitore et al., 2002; Reeder et al., 2001; Reeder et al., 2000; Sturchio et al., 1998). However, the phase association and speciation of U in marine carbonate rocks and unlithified carbonate sediments are poorly constrained because low U concentrations complicate X-ray absorption spectroscopic characterization. Experiments show that U is mostly negatively charged at seawater pH, and Ca-uranyl^{6+}-triscarbonato complexes, e.g., $CaUO_2(CO_3)_3^{2-}$, are the predominant species in modern oceans (Fig. 1). The latter can be incorporated in aragonite crystals without a significant coordination change whereas a significant disruption of the local structure occurs during U^{6+} incorporation into calcite (Reeder et al., 2001; Reeder et al., 2000). Hence, the U concentration in aragonite is typically around the Ca:U molar ratio of the parent solution, whereas the U concentration is lower in calcite. This property has been observed to lead to the rejection of U from the crystal structure during diagenetic neomorphism from metastable aragonite to stable calcite (Chen et al., 2018). In terms of oxidation states, U^{4+} has been identified in natural calcite samples and in limestones of Pleistocene-Neogene age, while U^{6+} has been documented both in calcites and modern coral aragonite (Kelly et al., 2003; Kelly et al., 2006; Pidchenko et al., 2013; Pingitore et al., 2002; Rasbury et al., 2021; Sturchio et al., 1998; Yuan et al., 2023).

The seawater $\delta^{238}U$ isotope value incorporated into primary carbonates during coprecipitation is, however, not mirrored in the buried sediment. Variable enrichments of ^{238}U relative to seawater have been observed in sediment profiles across modern carbonate depositional systems. For example, Chen et al. (2018) compiled U isotope data from Bahamas platform drill cores and found that early diagenetic carbonates have an average $\Delta^{238}U_{water\text{-}sediment}$ offset of 0.27 ± 0.14 ‰ (1SD) indistinguishable from modern carbonate sediments collected from the beach (Romaniello et al., 2013). Additionally, progressive downcore U enrichment is observed along with a $\delta^{238}U$ value positively offset from seawater immediately at and below the sediment–water interface (SWI) in several examples of active carbonate depositional systems (Bura-Nakić et al., 2020; Chen et al., 2018; Romaniello et al., 2013). The propagation of such a variable signal into lithified carbonate rock adds significant uncertainty to paleo-seawater $\delta^{238}U$ reconstructions, since the $\delta^{238}U$ value of bulk sedimentary carbonate carries a systematic, variable offset from overlying seawater; impossible to correct for through additional sampling (del Rey et al., 2020). These isotopic enrichments are typically attributed to reduction and isotopic fractionation of porewater U during syndepositional diagenesis occuring contemporaneously with or just after sedimentation while the sediments are unconsolidated and water-rich (Bura-Nakić et al., 2020; Chen et al., 2018; Romaniello et al., 2013; Zhang et al., 2020). The paleoredox community has attempted to overcome this challenge through a variety of measures such as mineralogy- and component specific analyses and leaches (e.g., Chen et al., 2022; Clarkson et al., 2020; del Rey et al., 2020; Hood et al., 2016; Tissot et al., 2018; Wang et al., 2022; Zhang et al., 2020). The dynamics of this enrichment, the speciation, oxidation state, cycling, and phase associations of U remain unconstrained, however, and $\delta^{238}U$ values have been observed to be both correlating and inversely correlating with downcore U enrichments, revealing a complex syndepositional-early diagenetic system of which we lack knowledge (e.g., Bura-Nakić et al., 2020; Romaniello et al., 2013).

In this study, we aim to further elucidate and understand the diagenetic phase- and redox cycling of U in marine carbonate systems using a new method to quantify U^{4+} and U^{6+} individually in modern and ancient carbonaceous sediments and rocks. We test an adaptation of a previously described ion-exchange chromatographic procedure to separate U^{4+} and U^{6+} fractions (e.g., Anderson, 1984; Anderson et al., 1989; Ervanne, 2004b; Stoliker et al., 2013; Wang et al., 2015) and employ it to quantify reduced and oxidized U fractions of carbonate- and surface-bound U, in a modern carbonate depositional environment and

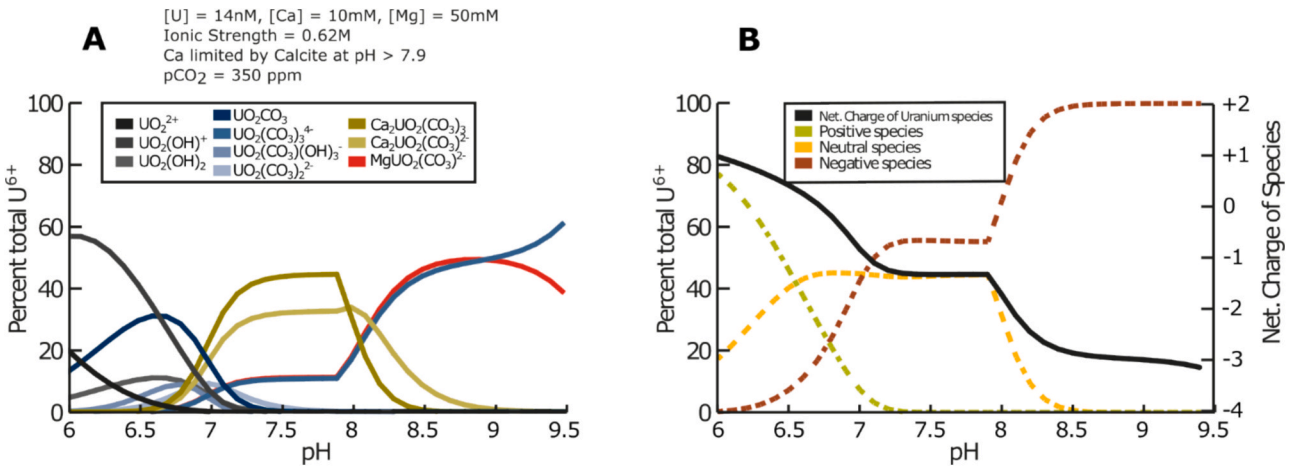

Fig. 1. The speciation of dissolved U in modern marine conditions is very sensitive to slight changes in pH which may affect the metal bonding, carbonation and charge of uranyl-carbonate species. The speciation diagram was calculated with PHREEQC software (Parkhurst and Appelo), using the sit.dat database and the most recent U thermodynamic data (Grenthe et al., 2004; Guillaumont et al., 2004; Dong and Brooks, 2006).

in a small sample set of Cambrian and Carboniferous carbonate samples. We then perform U L_3 HERFD-XANES spectroscopic measurements in natural marine carbonate sediments at natural, ~few ppm, U-level that could provide a more direct measure of the average oxidation state of total U in the samples and compare the results.

2. Methods and Materials

2.1. Sample sites

2.1.1. Environmental settings at Malo Jezero

Malo Jezero (small lake) is a seawater-fed lake on the island Mljet on the Croatian Adriatic coast (Fig. 2). It is characterized by supporting active carbonate deposition under a seasonally stratified marine saline water column, persistently oxic, with variable O_2 levels from fully oxic through hypoxic conditions in the bottom waters (Benociv et al., 2000; Sondi and Juračić, 2010). The lake has a maximum depth of ~ 30 m with minor tidally driven water exchange with the Adriatic Sea through a small channel connecting it first with lake Veliko Jezero (large lake), then the ocean. In the early summer, pH values increase while increased organic matter respiration and evaporation drive the development of thermal stratification with lower dissolved O_2 content in bottom waters. In the past, sulfidic conditions prevailed in the bottom waters but have not been documented for several decades. Chalcophile trace element (incl. Mo, Cd and Tl) enrichments at sediment depths greater than 17 cm likely reflect this period (Bura-Nakić et al., 2020; Sondi and Juračić, 2010; Sondi et al., 2017). Today, sediments of the deepest part of the lake contain 1–2 wt% total organic carbon and become anoxic immediately below the sediment–water interface (Bura-Nakić et al., 2020; Živković et al., 2023).

The total carbonate content of Malo Jezero sediments is more than 70 %, slightly decreasing with depth, with significant carbonate

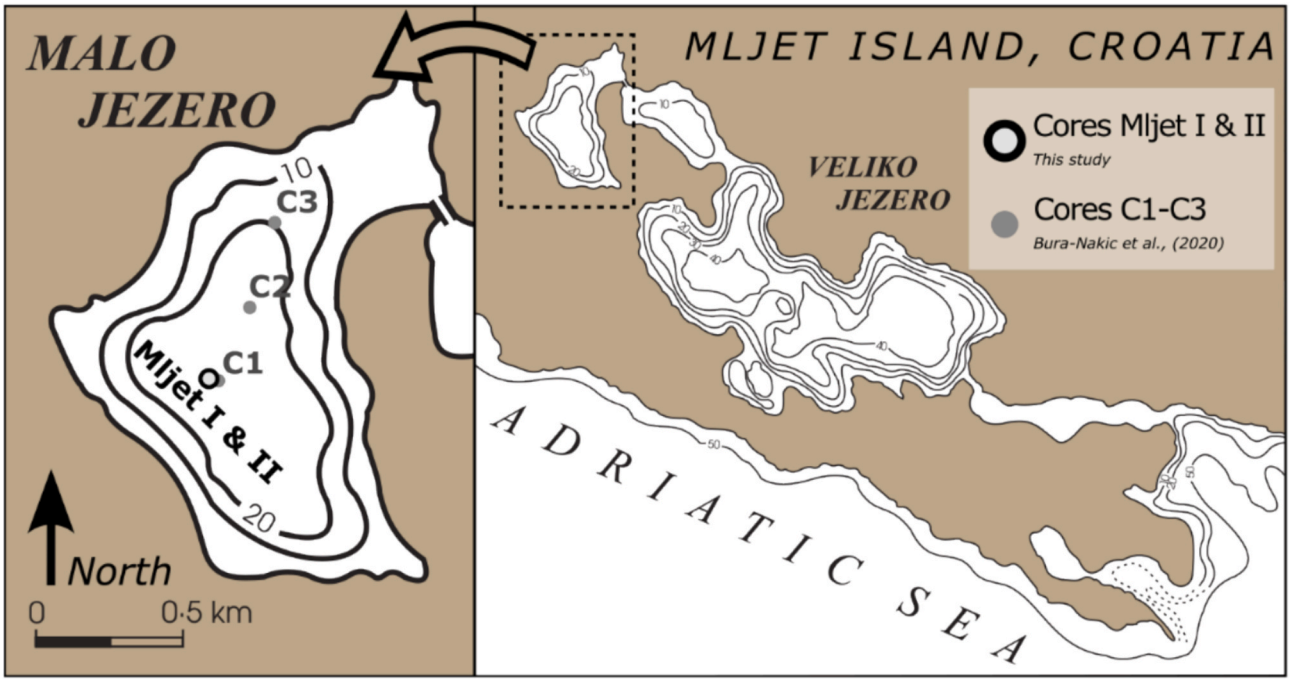

Fig. 2. Map of Malo Jezero on Mljet Island, with the sampling locations of the Mljet I and II cores (this study and Zivkocic et al., 2023, 42° 46′51″N, 17°20′57″E) and the C1-C3 cores (Bura-Nakić et al., 2020).

recrystallization, high Mg-calcite dissolution, and aragonite preservation (Lojen et al., 2010). Several sources of sediment carbonate have been identified. (1) Aragonite needles precipitate inorganically in the water column during biologically induced whiting events and aragonite constitutes ~ 55–70 % of all carbonate in the sediments with ~ half as much calcite (aragonite/calcite ratios ranges from 1.2 to 2.4) (Lojen et al., 2010; Sondi and Juračić, 2010). (2) The remaining carbonate is detrital calcite and dolomite derived from surrounding source rocks, as quantified from XRD analyses (Sondi and Juračić, 2010). The detrital carbonate content is also illustrated by $^{234}U/^{238}U$ activity ratios, $(^{234}U/^{238}U)_{act}$, scattered between that of seawater/lake water (1.137) and secular equilibrium (≈1.000), although difficulties in constraining U sources with this method challenges precise quantification since local soils with elevated $(^{234}U/^{238}U)_{act}$ also drain into the lake (Bura-Nakić et al., 2020). Previous studies have suggested downcore enrichments in ^{234}U to be an artifact of historical water-mass restriction and associated sulfidic conditions in the lake (Bura-Nakić et al., 2020).

Recent investigations of trace metal diagenesis in the deepest part of Malo Jezero show that metal respiration is the dominant metabolic pathway in the very surficial sediments (0–2 cm), followed by sulfate reduction immediately below (Fig. 3, Bura-Nakić et al. (2020); Živković et al. (2023)). In two out of the three sampled cores, U concentrations decrease from 14-15 nM in the bottom waters to 5–8 nM in porewaters at ~ 3 cm depth. This strong gradient in porewater U content witnesses periodically active removal of U inside the sediments, driving a diffusive flux of seawater U into the sediment porewaters.

The Malo Jezero sediments used in this study were cored from 2007 to 2010 (cores C1-C3, previously described with respect to U by Bura-Nakić et al. (2020)) and in 2021 (Core Mljet I, as described by Živković et al. (2023)). All cores C1-C3 were sectioned under a nitrogen atmosphere in a glove box immediately after sampling. Cores C1, C2 and C3 are from water depths 30 m, 22 m, and 13 m respectively. Porewater was removed by centrifugation and the remaining sediments were freeze-dried and stored until analysis. Core Mljet I was collected from 30 m water depth and stored frozen with in-situ porewater. For the separation of U oxidation states, core Mljet I samples were partitioned into 2 aliquots inside an anaerobic chamber in Copenhagen, one was analyzed anaerobically and wet (B1), and one was dried aerobically in an oven before analysis (B2).

2.1.2. Ancient sedimentary carbonate rocks

Carbonate rocks from Cambrian and Mississippian marine deposits were selected for oxidation state analysis by both anaerobic extraction and HERFD-XANES analyses.

Cambrian argillaceous limestone samples WH1-16 and WH1-24 were taken from the Paibian stage of the Mt Whelan #1 drill core (68.25 m and 93 m depth, respectively) through the Georgina Limestone Formation in Queensland, Australia (Greene and Balfe, 1980). These samples are laminated micrites from around the peak of the Steptoean Positive Carbon Isotope Excursion (SPICE) event with ~ 50 % of the U retained in the non-carbonate fraction of the sediments, incl. clay minerals (Dahl et al., 2014). Core sections had visible secondary veins removed with a water-cooled saw and the surfaces were leached with 2 M HCl, dried, crushed in a shatter box, ground to a fine powder with an agate mill and stored until analysis (Dahl et al., 2014).

Mississippian (upper Visean) samples were collected in May 2019 from roadcut outcrops of the Dian-Qian-Gui-Xiang carbonate platform on the Paleo-tethyan margin of Yangtze land in Guizhou, China,. Sample KPO19048 is a lime mudstone with abundant mm-sized brachiopod fossils collected 10 cm below a unit-wide paleokarst feature from the proximal platform Yashui section. Sample KPO19061 is a fossiliferous and lithoclastic packstone collected from the distal platform Naqing section. The Yashui and Naqing sections are more closely described by Chen et al. (2016a). The samples were powdered using a Dremel microdrill with titanium drill bits, cleaned thoroughly with MQ water and ethanol in between samples.

2.1.3. Reference materials

Repeated experiments with selective leaching followed by ion-chromatographic separations of tetravalent U^{4+} and hexavalent U^{6+} were performed on the modern argillaceous limestone NIST SRM-1d and a modern Atlantic Scleractinian aragonite coral (Coco-1) from the collection of the Natural History Museum of Denmark. Bothb materials are well characterized in terms of their U isotope compositions (e.g., Clarkson et al., 2021; Clarkson et al., 2020; Dahl et al., 2017; del Rey et al., 2020). The $\delta^{238}U$ value of the coral is indistinguishable from seawater (Livermore et al., 2020) and the carbonate associated U (U_{CAU} determined by an overnight 50 °C, 10 % acetic acid leach) in SRM-1d has a $\delta^{238}U_{CAU} = -0.11 \pm 0.04$ ‰ (Dahl et al., 2017). These materials are in-house reference materials as they have not been certified nor characterized for their U oxidation state. The carbonate fraction in SRM-1d likely constitutes a mixture of U^{4+} and U^{6+} given its positively fractionated $\delta^{238}U$ value relative to modern seawater, whereas Coco-1 most likely contains pure U^{6+} as do other modern aragonite corals (Kelly

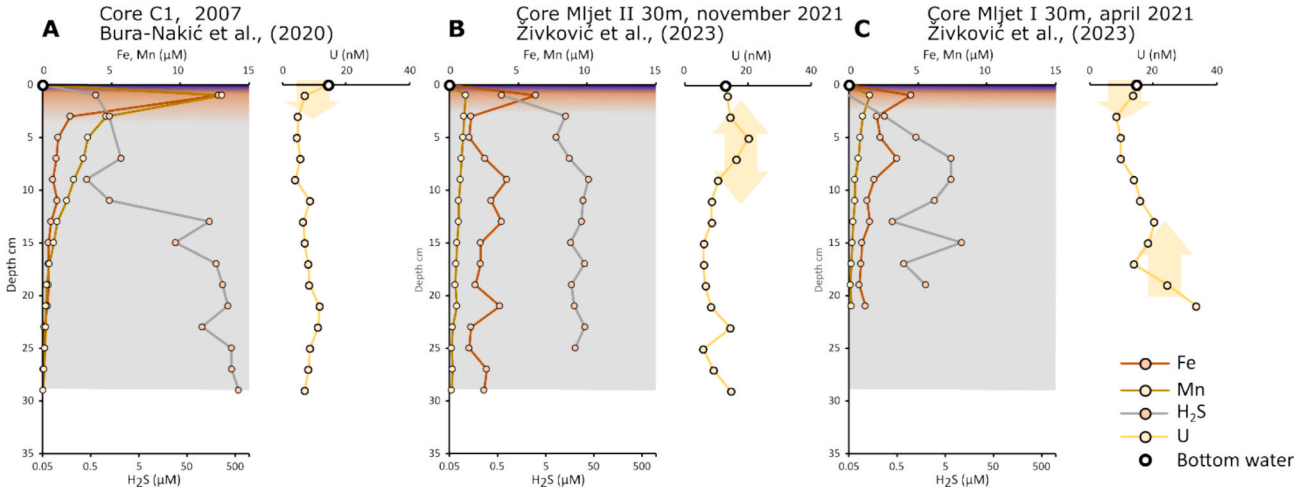

Fig. 3. Pore fluid concentrations of Fe, Mn and U in Malo Jezero sediments from three distinct cores, A) Core C1 (Bura-Nakić et al., 2020), B) Mljet II (Živković et al., 2023), and C) Mljet I (Živković et al., 2023). Cores Mljet I and II were collected at the same location in April and November 2021, respectively. Approximate interpretations of respiratory zones within sediments are colored blue (aerobic), reddish (metal-reduction) and grey (sulfate reduction). Interpretations of U diffusive gradients and direction of diffusion are denoted with yellow arrows of arbitrary scale.

et al., 2003; Pingitore et al., 2002).

2.2. Leaching and ion-chromatographic separation of U^{4+} and U^{6+} fractions in carbonate samples

2.2.1. Anaerobic laboratory environment

All leaching and separation procedures were carried out inside an anaerobic chamber (Coy Laboratory Products, type A) to minimize the possibility of U oxidation through contact with oxidizing solutions and air. The chamber atmosphere was 5.0 grade N_2 gas continuously maintained at < 10 ppm O_2, 50 % humidity, and free of hydrogen sulfide gas. All acids and MQ water used at redox-sensitive steps were purged with N_2 gas for ~ 30 min and equilibrated with the chamber atmosphere for a minimum of 48 h prior to contact with sample material.

2.2.2. Carbonate selective leaching protocols and bulk digestions protocols

We adopted a 0.5 M HCl leaching technique to selectively dissolve carbonate and authigenic reactive phases while minimizing the extraction of detrital phases, such as recalcitrant organics, clays and other non-carbonates. Similar selective leaching protocols have previously been used for isotope studies of carbonate-associated U and shown to extract mostly carbonate-bound U (e.g., Clarkson et al., 2020; Dahl et al., 2014). The aim of this procedure was to (1) extract authigenic U in a matrix suitable for subsequent ion chromatographical separation, and (2) to retain a representative $(U^{4+}/U^{6+})_{authigenic}$ ratio and minimize procedural oxidation, rather than ensuring 100 % yields of carbonate dissolution.

Two different approaches were used to prepare samples for leaching. For Cores Mljet I, C1-C3, and ancient samples, the sample materials were either freeze-dried (C1-C3) or oven-dried and powdered before analysis. Additionally, for Core Mljet I, frozen wet sample material, kept undisturbed and anoxic since sampling, was thawed and analyzed without drying and powdering. For these wet analyses, dry-basis concentrations were calculated by normalizing to the water content, as measured on equivalent sediment splits from a core collected simultaneously at an adjacent location. The water content of the samples ranged from 43–50 wt%, which, when considering the sample mass and acid volume used, dilutes the 0.5 M HCl to no less than 0.499 M HCl. Samples were weighed off to 5–200 mg and leached in a 5–10 mL solution of 0.5 M HCl (diluted from 37 % reagent grade, with MQ water) and 0.8 % L (+)-ascorbic acid (99–100.5 % USP grade) to inhibit oxidation of U^{4+} by dissolved Fe(III). The acids were mixed immediately prior to leaching to avoid degradation of the ascorbic acid (Golubitskii et al., 2007). Samples were vortexed immediately after acid addition to ensure complete mixing, and the residue was allowed to settle before pipetting out an aliquot of the supernatant for U^{4+}-U^{6+} separation. The resin itself acted as a filter, removing any fine particles that were not completely settled out at the time of pipetting. The total extraction time from the samples' first contact with acid to supernatant removal and loading onto the ion chromatographic column was 15 min.

The total U concentration in samples were measured in a third aliquot of samples from the Mljet 1 core. Sediment was freeze-dried and ~ 200 mg was digested in a 3 mL mixture of HNO3, HF and HCl in a 3:2:1 ratio. The samples were digested at 200 °C for 30 min in a CEM Mars 6 microwave system. After subsequent cooling, 10 mL of 4 % boric acid was added, and the samples were microwaved again for 15 min at 170 °C. The supernatant was then removed and diluted for mass spectrometric analysis.

2.2.3. U^{4+}- U^{6+} ion-chromatographic separation and analysis

A new ion-exchange procedure using the TEVA resin (Horwitz et al., 1995) was modified from previous work to determine the relative abundances of U^{4+} and U^{6+} fractions in both modern sedimentary and geological calcium carbonate matrices (Ervanne, 2004b; Hussonnois et al., 1989; Pidchenko et al., 2013; Răileanu and Cecal, 2008; Stoliker et al., 2013). A volume of 1 mL TEVA resin (50–100 µm, Eichrom Technologies), washed 10x with MQ-water, was loaded into HCl-pre-cleaned BioRad chromatography columns. The resin was further cleaned by washing with 10 mL of 0.1 M HCl and conditioned with 10 bed volumes of 4 M HCl. Sample leachates in 0.5 M HCl with ascorbic acid were immediately acidified to 4 M HCl using a 10 M HCl solution, shaken gently, and a 6 mL aliquot was loaded on the column. First, reduced U^{4+} was eluted along with ascorbic acid, Ca and most other elements with an additional 10 mL 4 M HCl. Hereafter, U^{6+} fractions were eluted with 10 mL of 0.1 M HCl. All eluents were collected in HCl- and HNO_3– cleaned Savillex Teflon beakers.

After the separation, the Teflon beakers were taken out of the anaerobic chamber and eluents were dried down on a hotplate under a HEPA-filtered atmosphere. All solutions were repeatedly treated with double-distilled concentrated HNO_3, and some with droplets of H_2O_2, to oxidize organic matter (mostly in the U^{4+} fractions where ascorbic acid was abundant). Ultimately, the solutions were dried down and redissolved in distilled ultrapure 2 % HNO_3 (NORMATOM®).

Concentrations of Al, Fe, Th, Ti, U and Zr of each separated fraction, and bulk digests, were determined in triplicate by Quadrupole Inductively Coupled Plasma Mass Spectrometry (ICP-MS) on an Agilent Technologies, USA, 7900 instrument at University of Southern Denmark. Measurements were performed using He collision cell technology and plasma suppression was corrected for by on-line addition of Sc, Rh and Ir to the sample flow as internal standards. The analytical precision, given as the average RSD of triplicate measurements across all samples, was 3.3 %, 1.9 %, 9.1 %, 7.4 %, 2.7 % and 8.1 % for Al, Fe, Th, Ti, U, and Zr, respectively. The accuracy of the mass spectrometer analysis is between 90 and 110 % for all elements considered here, as estimated from the long-term reproducibility of sediment reference materials MESS-4 and NCS DC73309 relative to their certified concentrations (Canfield and Naemi, 2025).

2.3. Experiments to assess the chemical separation method

Two experiments were carried out to (1, subsection 2.3.1) confirm the capacity of the TEVA resin to separate U^{4+} and U^{6+} at different HCl molarities, (2, subsection 2.3.2) quantify U oxidation by dissolved Fe^{3+} under anaerobic experimental conditions and relevant leaching timescales, and (3, subsection 2.3.2) assess relevant redox effect of Fe(III)-complexation by ascorbic acid and polyacrylic acid to prevent Fe(III)-induced U oxidation during the leaching procedure.

2.3.1. TEVA resin affinity

The TEVA resin affinity was confirmed by employing the anaerobic U^{4+}-U^{6+} extraction protocol (Section 2.2.3) on gravimetric U^{4+}-U^{6+} mixtures across a range of known U^{4+}:U^{6+} ratios, using the same pre-treatment, column cleaning, load- and elution volumes. This experiment confirms that the separated U aliquots are quantitatively eluted from the resin.

Solutions with known U concentrations and oxidation states were prepared from a Certiprep U ICP standard, assumed to be completely oxidized, i.e. hexavalent U. The U^{6+} was reduced to U^{4+} with $Ti(III)Cl_3$ in a 4 M HCl solution. The Ti(III)-U^{4+} solution was acidified to 10 M HCl and Ti(III) was quantitatively removed by ion chromatography on a 1 mL TEVA-loaded column (Saito, 1984). U^{4+} was eluted with 4 M HCl. Five mixtures of U^{4+} and U^{6+} were made from the U^{4+} solution and the original U^{6+} ICP solution giving 0 %, 25 %, 50 %, 75 %, and 100 % U^{4+}, respectively. Each mixture was loaded on a new, pre-cleaned TEVA column following our U^{4+} and U^{6+} separation protocol.

2.3.2. Inhibition of Fe^{3+}-mediated oxidation of U^{4+}

Oxidation of U^{4+} by Fe^{3+} is thermodynamically viable in strong acidic solutions, whereas Fe^{2+}-mediated reduction of dissolved U^{6+} is not (Du et al., 2011). Therefore, HCl-liberated Fe^{3+} from samples is a potential procedural oxidant, possibly causing an unsystematic bias lowering the measured U^{4+}:U^{6+} ratios. Several organic acids have been

proposed as selective Fe^{3+}-reducing agents, incl. ascorbic acid (Gavini et al., 1987; Korkisch et al., 1958), polyacrylic acid, lactic acid, and propionic acid (Ervanne, 2004a).

To assess the oxidative effect of Fe^{3+} on U^{4+} and the viability of different compounds to inhibit this oxidation we incubated U^{4+} with $Fe^{3+}Cl_3$ dissolved in 4 M HCl in various U:Fe molar proportions in the presence and absence of ascorbic acid or polyacrylic acid. In all cases, the U-Fe mixtures were allowed to equilibrate with the antioxidant for 15 min inside an anaerobic chamber. Tetravalent U was produced as outlined in section 2.3.1. $Fe^{3+}Cl_3$ was used as reagent grade, ascorbic acid in 99–100.5 % purity, and polyacrylic acid with an average molecular weight of 5,000. The antioxidant occurred in more than 2.5 times molar excess of the oxidant, Fe^{3+}, in all solutions. Loading of the incubation solutions on TEVA columns separating U^{4+} from U^{6+} marks the end of the 15-minute reaction time.

2.4. Estimating the U oxidation state using High-Energy Resolution Fluorescence-Detected X-ray Absorption near Edge Spectroscopy (HERFD-XANES) at the U L_3 edge

Synchrotron-based HERFD-XANES spectroscopy is a sensitive technique to determine oxidation state and bonding geometry of U in various materials. Conventional XANES spectroscopy have been applied to environmental samples typically with > 100 ppm U (Le Pape et al., 2020; Morin et al., 2016; Stetten et al., 2018) and rarely at the ppm level (Pingitore et al., 2002; Reeder et al., 2000). Uranium L_3 edge HERFD-XANES spectroscopic measurements for this study were performed at the Rossendorf beamline (BM20) at European Synchrotron Radiation Facility in Grenoble, France using the method described in Prieur et al. (2025) and Scheinost et al. (2021).

In the applied HERFD setup, an x-ray emission spectrometer (Kvashnina and Scheinost, 2016) with 0.5 m bending radius and Si(220) crystal analyzers were employed for data collection to reduce the line broadening (Kvashnina et al., 2014, 2015). HERFD measurements were achieved by scanning incident energy near the U L_3 edge and collection intensity at the maximum of the U L_{a1} emission line. The synchrotron delivered a photon flux of $2{\cdot}10^{11}$ sec^{-1} and the current in the storage ring was 200 mA during the analyses. The incident energy was selected using a double-crystal monochromator with Si(111) crystal. The total energy resolution was found to be 3.2 eV and was measured at half width half maximum of the elastic peak. Fluorescent photons were collected using a Ketek Silicon Drift Diode (SDD).

For the analyses, powdered carbonate rock samples were packed under ambient conditions in a 2 mm thick cardboard sample holder equipped with six sample slots and covered with 8-μm Kapton tape as windows. Samples were analysed under atmospheric conditions, hence O_2 diffusion into the sample could have occurred either during sample preparation and/or during the ~ 8 h of analysis. Moreover, prior to the measurements, fast time-scan tests were performed by collecting intensity at the maximum of U L_3 edge of uranyl compound in 0.1 s per point for 120 s. No evidence of beam damage was observed. The U L_3 edge HERFD-XANES spectra were compared to fresh, macrocrystalline UO_2 as a U^{4+} reference material and there was no drift in the energy scale through the analytical session. The UO_2 reference was made by pressing industrially obtained uranium dioxide powder into a pellet followed by sintering at 1700 °C under a H_2 /Ar stream. The industrial uranium dioxide, in its turn, was obtained from UF_6 by the gas-flame method, followed by annealing under reducing conditions at 600–650 °C (Gerber et al., 2021). The HERFD-XANES spectra of UO_2 aligned with previous studies of freshly produced UO_2 and not with its oxidation products U_4O_9, U_3O_7, and U_3O_8 (De Bona et al., 2022; Kvashnina et al., 2014). Hence, we rule out that the U^{4+} reference had been oxidized prior to or during analysis. Reliable XANES spectra were collected for samples with U concentrations ≥ 1.2 ppm.

The Iterative Transformation Factor Analyses (ITFA) algorithm was used to estimate component concentrations (Rossberg et al., 2003; Rossberg et al., 2009) by fitting spectra to the following solid state reference materials with distinct U oxidation states and coordination environments: $U^{4+}O_2$, $U^{6+}O_3$, $U^{6+}O_2(NO_3)_2{\cdot}6H_2O$ and $U^{5+}(H_2O)_2(U^{6+}O_2)_2O_4(OH)(H_2O)_2$. The fitting range was 17155–17190 eV or 17155–17200 eV. Errors on the relative concentrations of individual components are calculated as part of the ITFA algorithm, using the Real Error Function and the secondary set of eigenvalues resulting from abstract factor analysis of the spectral dataset (Malinowski, 1977; Rossberg et al., 2003). The data quality of the U^{6+} and U^{4+} proportions was evaluated based on the deviation of the sum of the fitted components from 100 %.

3. Results

3.1. Separation Technique

Separations of gravimetric mixtures of U^{4+} and U^{6+} demonstrate that the anaerobic separation technique faithfully reproduces U^{4+}/U^{6+} ratios with quantitative recovery from simple HCl matrices (Fig. 4).

Incubations of U^{4+} with dissolved Fe^{3+} show that partial oxidation of HCl-liberated U^{4+} occurs within the 15-minute leaching timeframe in solutions with molar Fe(III):U^{4+} ratios of 100–1000 or higher (Fig. 4). In this timeframe, we observe that up to 15 % of the original U^{4+} is oxidized to U^{6+}. The addition of ascorbic acid to the incubations effectively inhibited Fe^{3+}-mediated oxidation, whereas the addition of polyacrylic acid did not.

The U oxidation state of the two reference materials as well as replicate analyses of two Mt. Whelan limestone samples (Table 1) show that the method unambiguously reproduces modern aragonite coral as pure U^{6+}, while geological sample materials are reproduced with an aggregate 2SD of ± 23 % U^{4+}. The relatively low reproducibility stems from two replicate analyses with low U^{4+} contents, whereas the tetravalent U fraction in the other three materials reproduced within ± 5 %.

3.2. Chemical separation of U oxidation states in modern and ancient carbonates

The anaerobic U^{4+} and U^{6+} extraction techniques reveal that between 6 % and 60 % of HCl extractable U reside in the tetravalent form in Malo Jezero carbonate sediments and ancient carbonate rocks. Across all samples the HCl leach extracted between 0.6 and 4.75 μg/g U (Table 2 & S1). Fig. 5 shows the concentration of U^{4+} and U^{6+}, with depth, of the Malo Jezero Mljet I core. There is a strong trend of increasing U^{4+} contents with depth and a slight systematic decrease in U^{6+} contents, in the sediment split that was kept and analyzed anaerobically and wet. Contrary, a constant and rather small fraction (~10 ± 5 %) of total HCl-leachable U resides as U^{4+} in the profile of the aerobically dried sediment split. On average, the U_{HCl} yields are comparable between the batches analyzed wet and dry, though the wet analyses yield higher concentrations in the upper part of the core, and the dry analyses yield somewhat higher concentrations in the deeper part of the core (Fig. 5C). Compared to bulk digests (HF + aqua regia), our dry HCl-leaches extracted between 16–40 % of the U and wet HCl-leaches extract between 21–59 % of the U. Some features in the depth profiles extend across all three extraction methods (wet and dry HCl-leaches and bulk digests), including positive inflections in U content at 5 and 9 cm depth, and negative inflections at 7 and 25 cm depth.

3.3. Uranium oxidation state determination using U L_3 edge HERFD-XANES spectroscopy

Independent analyses of the oxidation state of total U in the samples is performed by HERFD-XANES analysis. Accumulated U L_3 edge HERFD-XANES spectra of five modern sediment samples from Malo Jezero cores 1–3 plus three geological samples from the Mt. Whelan drill core, Yashui and Naqing sections are shown in Fig. 6 together with

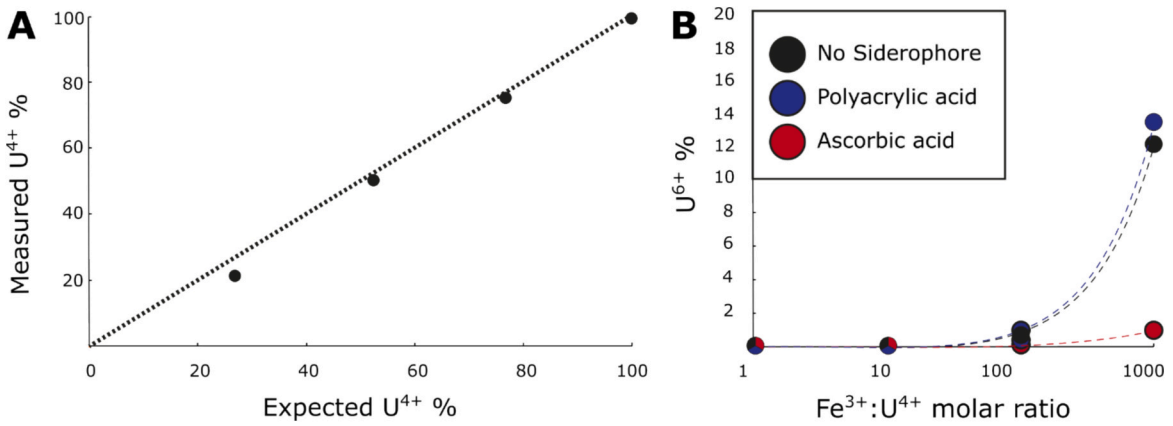

Fig. 4. Experimental assessments of the efficacy of the U^{4+}-U^{6+} separation protocol. Analytical uncertainties (2SE) confined within datapoints. **A**) Gravimetric mixtures of U^{4+} and U^{6+} in an HCl matrix are accurately reproduced from separations on the TEVA resin. The line of equality is shown as a dotted line. **B**) Addition of the siderophore ascorbic acid to sample leaches effectively inhibits oxidation of U^{4+} by liberated Fe^{3+}, as opposed to addition of polyacrylic acid and control experiments. Typical Fe:U ratios in carbonate rocks and sediments of 1000 and more may pose significant risk of procedural U oxidation.

Table 1
Overview of replicate analyses of samples and blanks, and detection limits. U_{HCl} contents and $(U^{4+}/U)_{HCl}$ ratios are given as means and standard deviations of replicate analysis populations.

Replicate material	**# of replicate analyses**	**U_{HCl}**	RSD	**U^{4+}/U_{HCl}**	2SD	2SE
		μg/g	%			
Coco-1	7	3.04	26	0.02	0.01	0.00
SRM 1d	5	1.09	18	0.36	0.31	0.14
WH1-16	2	0.68	116	0.23	0.09	0.07
WH1-24	2	0.59	3	0.45	0.17	0.12
					Weighted 2SD	0.23
					Weighted 2SE	0.12

Blanks	**# of replicate analyses**	**U**	**Detection limits**	
		pg		*ng/g*
Procedural Blank	7	51–455 (mean = 188)	HCl leaches	0.6
HCl blank	3	< 14	Bulk digests	1.3
Ascorbic acid blank	2	< LOD		

< 9.6 % of most dilute sample

reference spectra of $U^{4+}O_2$, $U^{6+}O_3$, and $U^{6+}O_2(NO_3)_2{\cdot}6H_2O$. Data quality on all samples is sufficient to resolve absorption peaks, except KPO19048 (0.74 ppm HCl-extractable U). Beam-induced reduction of U^{6+} is excluded on the basis that we observed no spectral changes during repeated scans over the U L_3 edge. Qualitatively, these analyses consolidate that U exists in several bonding environments and likely in multiple oxidation states. The differences between U^{6+}-uranyl and alpha-$U^{6+}O_3$ (no uranyl) reference spectra in terms of both wavelength of absorption peak and post-peak shoulder features, shows that the local bonding environment of U also affects the U L_3 HERFD-XANES spectra. The effect of ligands may complicate quantitative determination of oxidation state, for example the broad post-peak shoulder at 17185–17190 eV is a feature characteristic of uranyl (i.e. axial U=O bonds). The $U^{4+}O_2$ reference has a distinct increase in absorption at energy levels around 17210 eV that is not observed in apparently U^{4+}-rich samples. This spectral dissimilarity between U^{4+}-rich samples and the U^{4+} reference material indicates that carbonate samples contain U^{4+} compounds that are not represented by our reference materials.

To assess the average U oxidation state in the samples, we performed two Iterative Transformation Factor Analyses (IFTA) of the sample spectra, assuming the spectra was composed of U^{4+} in uraninite-form, and U^{6+} in either α-UO_3 or uranyl-form; i.e. $U^{6+}O_2(NO_3)_2{\cdot}6H_2O$. This simplification led to tentative estimates for the proportion of tetravalent U^{4+} and hexavalent U^{6+} in all samples (Table 3). All samples but the surficial (C1_0_2 and C2_0_2) appear to contain both U^{4+} and U^{6+} in variable proportions, and the differences in U^{6+} contents between analyses using α-UO_3 and uranyl as the U^{6+} reference are close to or within uncertainty. We also explored the effect of including a pentavalent U^{5+} phase in a 3-component ITFA analysis (Table 4). Estimated proportions of U^{4+} and U^{6+} change significantly when pentavalent U is included in the analyses, drastically lowering U^{4+} contents of C1_0_2 and C2_0_2. However, we note that differences between pentavalent and hexavalent U phases are not resolvable on U L_3 edge spectra (Ikeda et al. 2017), leaving this result inconclusive.

Most samples show a positive correlation between HERFD-XANES and chemical extraction U^{4+} estimates, however, on a trend significantly above the 1:1 correspondence line (Fig. 7). Multiple factors may contribute to this offset, including 1) the presence of a U^{4+} phase in the samples that is not extracted by 0.5 M HCl leaching (e.g. clay/mica, organic matter), 2) a partial procedural oxidation associated with the anaerobic leaching protocol not seen when applied to Fe-doped reference materials, and 3) abundance of pentavalent U phases either appearing as U^{4+} in the XANES fit or reacting to hexavalent U in the extraction procedure.

The two top-core samples (0–2 cm depth) from cores C1 and C2 display a conspicuously large discrepancy between HERFD-XANES ITFA fits and anaerobic chemical extractions, yielding 96–100 % of total U in the samples as tetravalent U^{4+} while anaerobic extractions show that HCl-leachable U contains only 9–12 % U^{4+}, respectively (Fig. 7).

4. Discussion

4.1. Ion chromatographic separation of U^{4+} and U^{6+}

4.1.1. Reference materials

We have designed and tested a new anaerobic chromatographic method to separate U^{4+} and U^{6+} from carbonate mineral samples that tolerably reproduces U^{4+}/U_{HCl} ratios in a series of in-house reference materials (Table 1). The method confirms expectations that a well-preserved modern aragonitic coral (Coco-1) contains exclusively

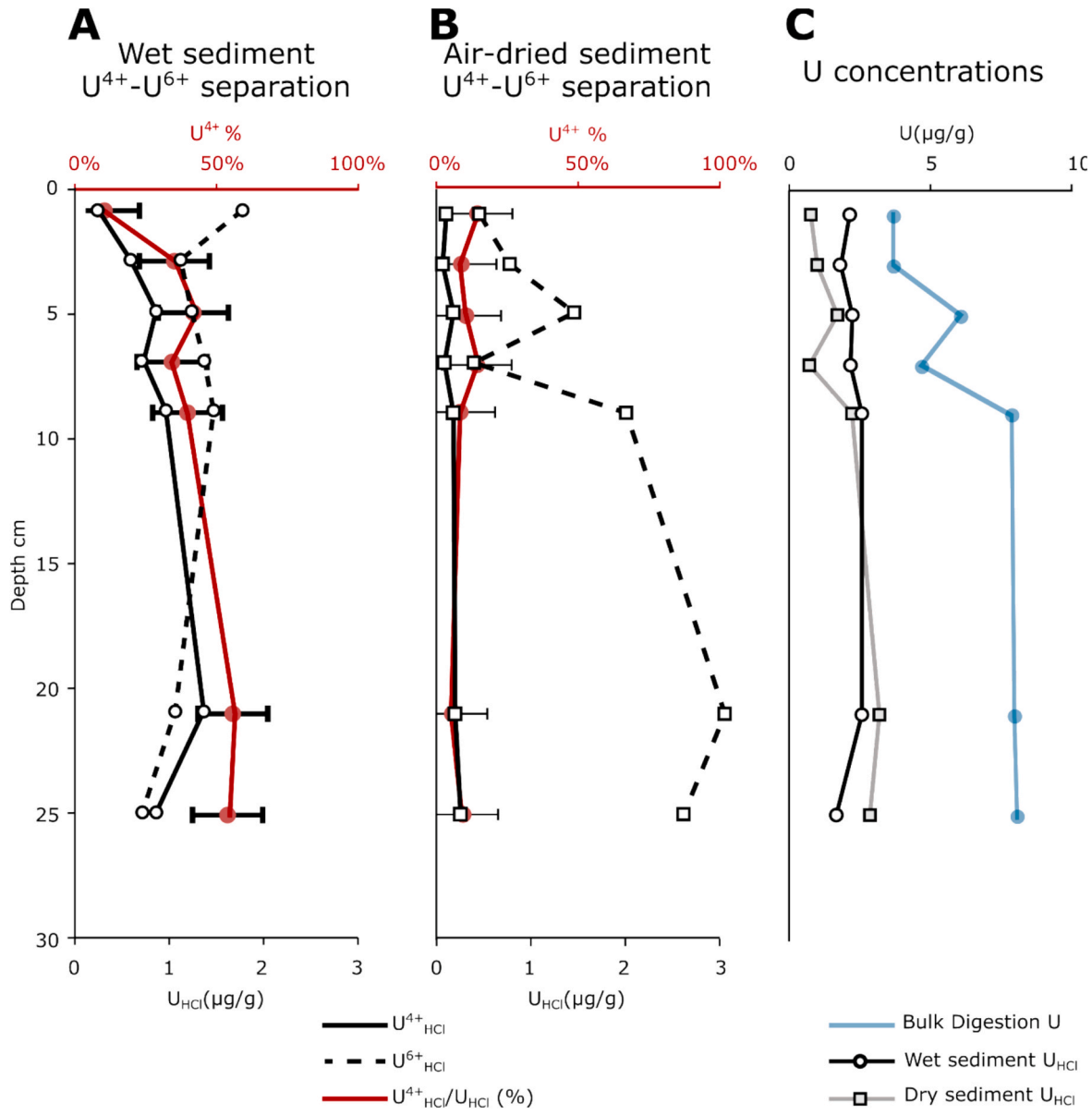

Fig. 5. Profiles of U species in sediments from the deepest part of Malo Jezero. Uncertainties given on U^{4+}/U_{HCl} ratios are the 2SE of the weighted average of repeat measurements given in Table 1. (A) In leaches and separations of the sediment split treated anaerobically, HCl-liberated U^{4+} accumulates with depth driving a downcore increase of the U^{4+}/U_{HCl} ratio. (B) In the sediment split that was oven-dried aerobically prior to analysis, nearly all U liberated is hexavalent U^{6+}. (C) Variations in total U leached with HCl from anaerobically and aerobically treated sediment splits are comparable, although more U is leached in shallow samples from 0-10 cm depth whereas the aerobic extraction yields more U from deeper samples below > 20 cm depth.

hexavalent U, and that modern and ancient marine carbonate sediments contain both U^{4+} and U^{6+} phases. In combination, these results also indicate that the low pH obtained during the 0.5 M HCl leach, does not in itself induce a reduction of U^{6+} to U^{4+}. On average, U^{4+}/U_{HCl} ratios reproduce within ± 0.12 (2 SE), however, considerable variability is observed for the in-house reference material SRM-1d as discussed below.

The WH1-16 argillaceous limestone was processed in duplicate with very distinct yields: U_{HCl} concentrations of 1.24 and 0.12 ug/g. The reason for varying yield likely lies with the acid to sample ratio and, thus, shorter contact time between sample and the acid (for WH1-16 replicates, we used 4.62 mg vs. 113 mg rock powder and 10 mL vs. 7.5 mL acid, respectively). Importantly, we note that the U^{4+}/U_{HCl} ratio remained consistent between these two extractions (2SD = 0.09), highlighting that quantitative U_{HCl} yields may not necessarily be a prerequisite for reliable U^{4+}/U_{HCl} determination.

The proportion of U^{4+} in repeated experiments of the argillaceous limestone SRM-1d varies considerably (2SD ± 0.31). The U^{4+}_{HCl} content of SRM1d replicates was compared with HCl leachable detrital indices Al, Th, Ti and Zr, and Fe_{HCl}, to assess whether variable leaching of auxiliary non-carbonate phases can explain the U^{4+}/U_{HCl} variability. Non-carbonate phases present in environmental samples might include (e.g. non-crystalline), reduced U hosted in organic compounds (Roebbert et al., 2021; Vettese et al., 2020) phosphate-associated U such as ningyoite $(U,Ca,Ce)_2(PO_4)_2{\cdot}1–2(H_2O)$, lermontovite $(U(PO_4)(OH)\bullet(H_2O))$, and autunite $(Ca(UO_2)_2(PO_4)_2\bullet 10–12H_2O)$ (Le Pape et al., 2020; Morin et al., 2016) and perhaps U associated with iron-oxides or clay-minerals (Dahl et al., 2014). The U^{4+}_{HCl} content of SRM1d weakly correlates with HCl leachable Fe and detrital indices, with p-values > 0.25. These correlations indicate that our leach, possibly due to the lack of a filtration step, partially and variably extracts U^{4+} from a non-carbonate phase in SRM1d. In summary, the in-house limestone references WH1-16, WH1-24 and SRM-1d reproduce $(U^{4+}/U)_{HCl}$ ratios with an average 2SE of

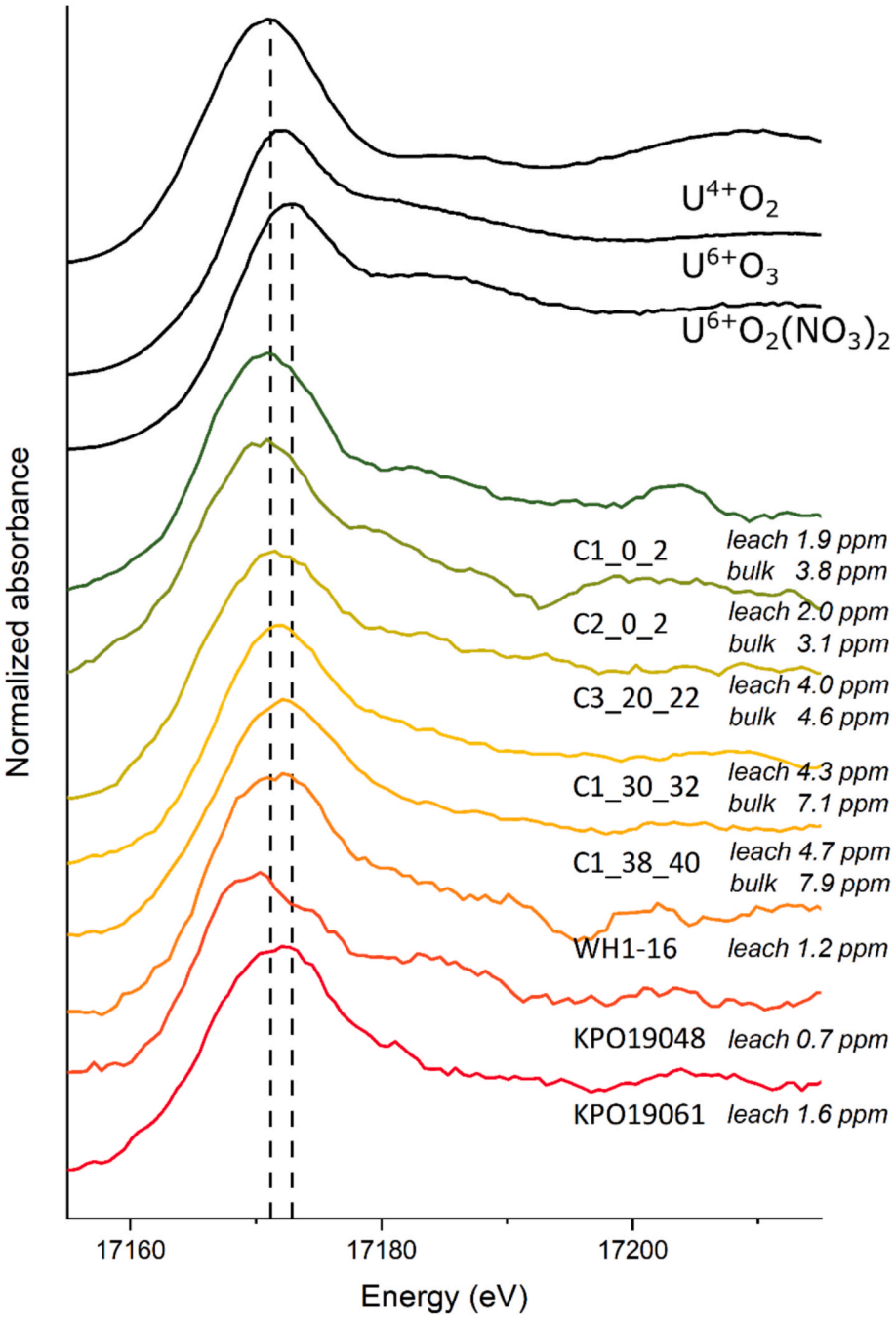

Fig. 6. Normalized U L_3 edge HERFD-XANES spectra of geological samples, dried carbonate sediments from Malo Jezero (Mljet I core), and selected relevant reference materials.

0.12. We use this 2SE as the uncertainty metric of U^{4+}/U_{HCl} ratios of all samples, aware of the caveats outlined above.

4.1.2. Uranium redox sensitivity

The oxidation experiments with fresh carbonate sediment elucidate the U^{4+} phases present in modern sediments, the possibility for procedural oxidation in the laboratory, and the redox-sensitive cycling of U in carbonate sedimentary environments. A comparison of a wet anaerobic extraction and an aerobic oven-dried extraction of Malo Jezero core Mljet I sediments demonstrated a greater proportion of reduced U in samples always kept strictly anaerobic (Fig. 5). Further, higher U^{4+} contents are observed at greater sediment depths as would be expected at lower redox potential in the pore fluids. This depth increase of U^{4+}_{HCl} is independent of any variable leaching of detrital compounds, as evidenced by depth-increasing ratios of U^{4+}_{HCl} normalized to HCl leachable Al, Fe, Th, Ti and Zr (Fig. S2). Reduced U is a minor component in sediments treated aerobically, and the U^{4+} contents remain constant at ~ 0.2 μg/g with depth. Hexavalent U is present at all sediment depths in both dry and wet samples. Thus, we infer that most reduced U is hosted in a labile, air-sensitive phase in fresh carbonate mud and that another more recalcitrant U^{4+} phase constitutes a minor component. This finding is consistent with recent evidence that microbial U reduction products are labile nano- and non-crystalline U^{4+} species that have been observed to oxidize and mobilize on short timescales, from days to weeks (Cerrato et al., 2013, Newsom et al., 2015, Stetten et al., 2018, Morin et al., 2016).

Table 2
Sediment- and rock samples studied with U concentration in HCl leaches and chromatographic separations.

Sample ID	Location	Age	Depth	Drying method	Air contact	U_{HCl}	U^{4+}/U_{HCl}	U_{total}	Sampling reference
			cm			*μg/g*	*Chromatography*	*μg/g*	
C1_0_2	Mljet Lake. Croatia	Modern	1	Freeze dried	Aerobic	1.93	0.09	3.84	Bura-Nakić et al.. 2020
C1_30_32	Mljet Lake. Croatia	Modern	31	Freeze dried	Aerobic	4.26	0.07	7.11	Bura-Nakić et al.. 2020
C1_38_40	Mljet Lake. Croatia	Modern	39	Freeze dried	Aerobic	4.75	0.06	7.9	Bura-Nakić et al.. 2020
C2_0_2	Mljet Lake. Croatia	Modern	1	Freeze dried	Aerobic	2.01	0.12	3.06	Bura-Nakić et al.. 2020
C3_2022	Mljet Lake. Croatia	Modern	21	Freeze dried	Aerobic	3.97	0.15	4.62	Bura-Nakić et al.. 2020
WH1-16	Mt. Whelan Drill Core. Georgina Limestone Formation. QLD. Australia	Cambrian			Aerobic	1.24	0.20	NA	Dahl et al.. 2014
WH1-24	Mt. Whelan Drill Core. Georgina Limestone Formation. QLD. Australia	Cambrian			Aerobic	0.60	0.51	NA	Dahl et al.. 2014
KPO_19061	Naqing. Guizhou. China	Mississippian			Aerobic	1.60	0.60	NA	This work
KPO_19048	Yashui. Guizhou. China	Mississippian			Aerobic	0.74	0.28	NA	This work
Mljet I B1_1	Mljet Lake. Croatia	Modern	1	No drying	Anaerobic	2.2	0.13	3.7	This work
Mljet I B1_2	Mljet Lake. Croatia	Modern	3	No drying	Anaerobic	1.8	0.35	3.7	This work
Mljet I B1_3	Mljet Lake. Croatia	Modern	5	No drying	Anaerobic	2.3	0.42	6.1	This work
Mljet I B1_4	Mljet Lake. Croatia	Modern	7	No drying	Anaerobic	2.2	0.34	4.7	This work
Mljet I B1_5	Mljet Lake. Croatia	Modern	9	No drying	Anaerobic	2.6	0.40	7.9	This work
Mljet I B1_6	Mljet Lake. Croatia	Modern	21	No drying	Anaerobic	2.6	0.56	8.0	This work
Mljet I B1_7	Mljet Lake. Croatia	Modern	25	No drying	Anaerobic	1.7	0.55	8.1	This work
Mljet I B2_1	Mljet Lake. Croatia	Modern	1	Oven dried	Aerobic	0.81	0.14	3.7	This work
Mljet I B2_2	Mljet Lake. Croatia	Modern	3	Oven dried	Aerobic	1.07	0.08	3.7	This work
Mljet I B2_3	Mljet Lake. Croatia	Modern	5	Oven dried	Aerobic	1.78	0.10	6.1	This work
Mljet I B2_4	Mljet Lake. Croatia	Modern	7	Oven dried	Aerobic	0.75	0.14	4.7	This work
Mljet I B2_5	Mljet Lake. Croatia	Modern	9	Oven dried	Aerobic	2.30	0.08	7.9	This work
Mljet I B2_6	Mljet Lake. Croatia	Modern	21	Oven dried	Aerobic	3.24	0.06	8.0	This work
Mljet I B2_7	Mljet Lake. Croatia	Modern	25	Oven dried	Aerobic	2.91	0.09	8.1	This work

Table 3
Iterative transformation factor analysis of XANES spectra with two components: U(IV) as UO_2 and U(VI) as either UO_3 or Uranyl $UO_2(NO_3)_2$. Fitting range 17,155–17,190 eV. Error estimates are calculated as part of the ITFA algorithm, using the Real Error Function, as described in section 2.4.

Sample ID	Combination between UO_2 and UO_3					Combination between UO_2 and Uranyl				
	UO_2		UO_3		Total	UO_2		Uranyl		Total
	fraction	±	*fraction*	±		*fraction*	±	*fraction*	±	
C1_0_2	0.96	0.04	0.00	0.04	0.96	0.96	0.03	0.00	0.03	0.96
C1_30_32	0.50	0.04	0.48	0.04	0.98	0.58	0.03	0.40	0.03	0.98
C1_38_40	0.52	0.04	0.48	0.04	1.00	0.60	0.03	0.40	0.03	1.00
C2_0_2	1.00	0.04	0.00	0.04	1.00	1.00	0.03	0.00	0.03	1.00
C3_20_22	0.63	0.04	0.42	0.04	1.05	0.70	0.03	0.35	0.03	1.05
KPO19061	0.89	0.04	0.12	0.04	1.01	0.91	0.03	0.10	0.03	1.01
WH1-16	0.71	0.04	0.29	0.04	1.00	0.76	0.03	0.24	0.03	1.00

Table 4
Iterative transformation factor analysis of XANES spectra to three components: UO_2, mixed valence U(V)-U(VI) (oxy)hydroxide $U^{5+}(H_2O)_2(U^{6+}O_2)_2O_4(OH)(H_2O)_2$, and Uranyl $UO_2(NO_3)_2$. Fitting range: 17,155–17,200 eV. Error estimates are calculated as part of the ITFA algorithm, using the Real Error Function, as described in section 2.4.

Sample ID	$(U^{4+}/U)_{HCL}$	U^{4+}		$U^{5+} - U^{6+}$		U^{6+}		Total
		fraction	±	*fraction*	±	*fraction*	±	
C1_0_2	0.09	0.75	0.04	0.20	0.02	0.05	0.05	1.00
C1_30_32	0.07	0.46	0.04	0.16	0.02	0.32	0.05	0.94
C1_38_40	0.06	0.38	0.04	0.31	0.02	0.27	0.05	0.97
C2_0_2	0.12	0.46	0.04	0.75	0.02	0.00	0.05	1.21
C3_2022	0.15	0.24	0.04	0.57	0.02	0.22	0.05	1.03
WH1-16	0.20	0.73	0.04	0.01	0.02	0.24	0.05	0.99
KPO_19061	0.60	0.48	0.04	0.57	0.02	0.00	0.05	1.05

Tetravalent U may be oxidized by dissolved Fe^{3+} even under $(Fe^{3+}/U^{4+})_{HCl}$ molar ratios of 1000 (section 3.1). Table 5 shows that Fe_{HCl} to U_{HCl} ratios were between ~ 2,500–11,300 during anaerobic leaches of Mljet I sediments, though likely only a fraction of the liberated iron was Fe^{3+}, since leaching of Fe oxides requires a reducing extractant and longer timescales (e.g., Poulton et al., 2005). Nevertheless, the oxidation of U^{4+} is effectively inhibited when ascorbic acid is present in molar ratios with Fe^{3+} of ~ 2.5 or higher (section 3.1). Higher molar ratios

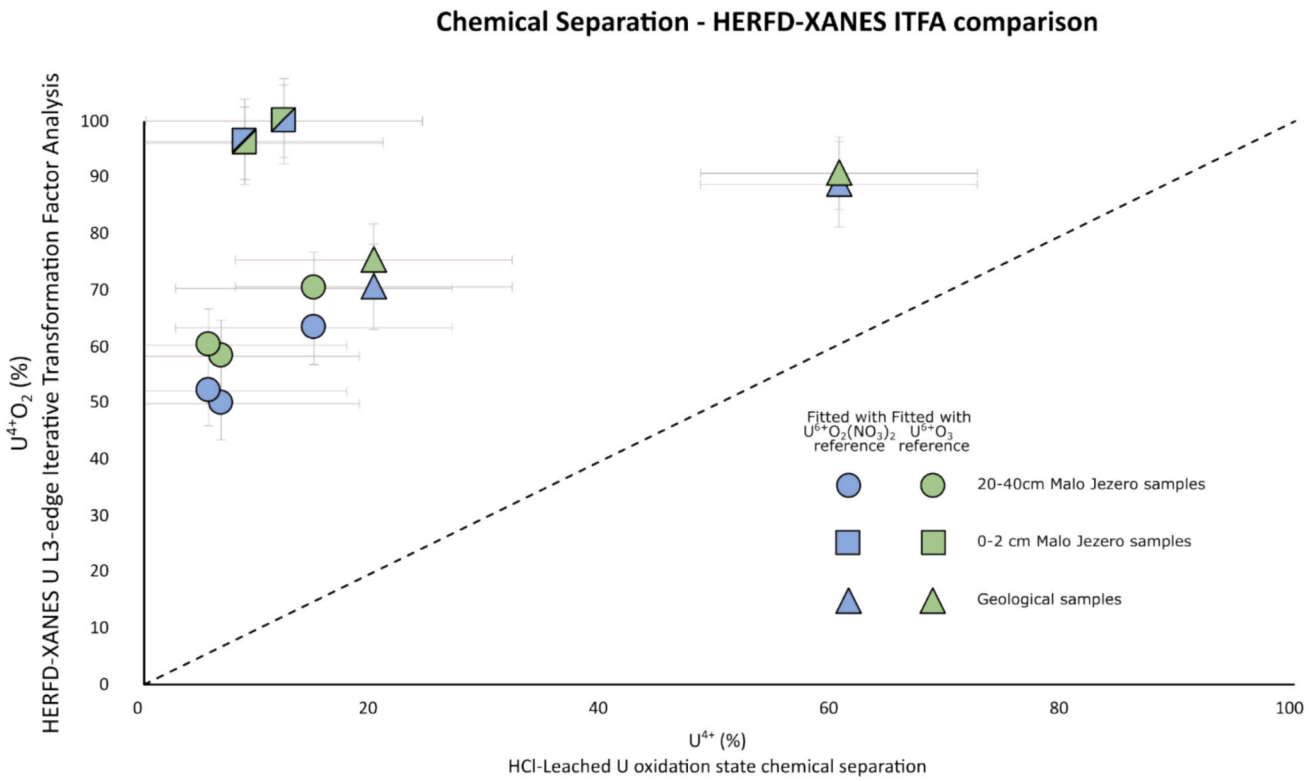

Fig. 7. Iterative Transformation Factor Analyses (ITFA) of sample U oxidation state from U L_3 edge HERFD-XANES spectra plotted against chromatographic separations of HCl extractable U^{4+} and U^{6+}. ITFA results using UO_3 and Uranyl as the U^{6+} reference component are shown in green and blue respectively. Error bars on ITFA results are calculated as part of the ITFA algorithm (section 2.4 and Table 3), while error bars on the chromatographic separation is the 2SE of in-house reference materials (section 4.1.1, Table 1). Most samples plot above the 1:1 line and show a higher proportion of U^{4+} from HERFD-XANES analyses than in recorded by the anaerobic extraction protocol of carbonate associated U. This can be mostly explained by the presence of U^{4+} phases not extracted by HCl. However, surficial sediments from Malo Jezero core C1 and C2 almost exclusively consist of U^{4+} according to the U L_3 edge HERFD-XANES spectra whereas anaerobic chromatographic analyses suggest carbonate associated U is mostly hexavalent. We infer that the estimated U oxidation state from U L_3 edge HERFD-XANES spectra depends on reference materials with similar coordination environment, and therefore may sometimes give erroneous results.

Table 5
Extraction yield (U_{HCl}), Fe/U and Ascorbic Acid/Fe ratio in the anaerobic HCl extraction.

Sample name	Sediment depth (cm)	U_{HCl} (µg/g)	Fe_{HCl} (µg/g)	Fe_{HCl}/U_{HCl} (molar ratio)	Ascorbic Acid/Fe_{HCl} (molar ratio)
Mljet I B1_1	1	2.17	4253	8314	6.0
Mljet I B1_2	3	1.88	5001	11,306	5.1
Mljet I B1_3	5	2.30	2616	4827	9.7
Mljet I B1_4	7	2.24	3627	6886	7.0
Mljet I B1_5	9	2.63	1872	3022	13.6
Mljet I B1_6	21	2.61	1507	2454	16.9
Mljet I B1_7	25	1.74	1367	3346	18.6

(6–19) were attained during the leaching and, thus, we find no evidence that $(U4+/U)_{HCl}$ ratios were altered through U oxidation by Fe^{3+} during anaerobic leaching of Mljet I sediments (Table 5).

4.1.3. Comparing chromatographic and spectroscopic U oxidation state analyses

The robustness of the U oxidation state measurements in modern and geological carbonate samples was assessed by comparing results from the anaerobic TEVA separation to the results obtained by HERFD-XANES spectroscopy. The energy of U L_3 edge (17176–17179 eV) provides a measure of the average oxidation state of total uranium in samples with similar ligands and coordination environment (Kosog et al., 2012), whereas our anaerobic ion chromatography procedure quantifies HCl-leachable U partially leached and separated into tetravalent and hexavalent forms from carbonate-containing samples. The comparisons were made with the two ancient carbonate rock samples and samples from the C1-C3 cores. Thus, only samples that were dried down, powdered and stored under aerobic conditions, prior to HERFD-XANES analysis and anaerobic extractions, are considered. Therefore, the samples applied for HERFD-XANES analyses likely underwent some oxidation prior to analysis. Since we use the same, potentially oxidized, samples for comparison to the chromatographical analyses, we consider them well suited for a comparison despite not reflecting their original sedimentary U oxidation state.

In most samples analyzed by both HERFD-XANES and our new anaerobic extraction method, we observe a positive correlation between the U^{4+} fraction in the HCl leach and the total UO_2 fraction estimated from bulk rock HERFD-XANES analyses. This correlation suggests that some U-phases have been accurately identified by both methods (Fig. 7). However, our HERFD-XANES analyses indicate significantly higher proportions of tetravalent U, representing 50–100 % of the total U in modern carbonate sediments and 70–90 % in geological limestone samples (Table 3). This is based on fitting the HERFD-XANES spectra with only hexavalent and tetravalent U reference materials. In contrast, anaerobic ion chromatography of the HCl-leachable fraction yields a much lower U^{4+} content—just 6–15 % for sediments and 20–60 % for limestone samples. The discrepancy is particularly large for Malo Jezero surface sediment samples (Fig. 7). We consider four possible causes contributing to the offset from the 1:1 linear correlation line.

First, tetravalent U phases, not extracted with a short leaching in 0.5 M HCl, could be present in the bulk samples, including crystalline and non-crystalline UO_2 hosted in clays, phosphates, oxide minerals, and detrital organic matter. Bura-Nakić et al. (2020) found that authigenic U

in Malo Jezero samples accounts for ~ 50 % of bulk U in the sediments with the rest in detrital phases. Their estimates of authigenic U concentrations and $\delta^{238}U_{auth}$ values were calculated as the deviation from a mixing line between the two local detrital endmember U_{bulk} concentrations and isotope signatures. Our U yields from 0.5 M HCl extractions correspond reasonably to their calculated authigenic U concentrations on the same samples (Table S2). In general, samples from core C1 match well while U_{HCl} concentrations in samples from cores C2 and C3 are higher than calculated U_{auth}. Hence, we infer that our HCl leaches has quantitatively extracted most authigenic U and, thus, the higher U^{4+} contents estimated with the HERFD-XANES method unlikely reflects an authigenic U^{4+} phase, but perhaps an allogenic (detrital) U phase that could not be extracted by HCl. If we assume that all residual U (not extracted by HCl) is tetravalent uranium; e.g., in the form of UO_2, then we should find 25–55 % UO_2 in the HERFD-XANES spectra. This is still less than calculated by fitting components to the observed spectra (50–100 %). Therefore, the presence of detrital U phases may influence the comparison of chromatographic and spectroscopic results, however the positive offset from the 1:1 line from all studied samples is beyond partial explanation by a U^{4+}-rich HCl-residue alone.

Secondly, we considered procedural oxidation during acid leaching and/or chromatographic separation. All samples were handled anaerobically during sample leaching, and ascorbic acid was added in excess of the reactive Fe concentration, which we have shown (section 4.1.2) effectively protects against U^{4+} oxidation by dissolved Fe^{3+} in the HCl-leaches. Moreover, U oxidation by manganese is not observed in a similar extraction procedure (Yuan et al., 2023). Although, we cannot completely rule out U oxidation with other redox-sensitive elements, we are not aware of a process that could have driven U oxidation in our leaching procedure.

Third, the lack of appropriate reference materials for the ITFA principal component analysis may contribute to the discrepancy between chromatographic and spectroscopic analyses. For instance, crystalline uraninite (UO_2) was used as the U^{4+} reference; however, as discussed in Section 4.2, the U^{4+} phases present are likely nano- or non-crystalline microbial reduction products, potentially uranium-phosphate complexes. Unlike uraninite and the uranyl ion, which are characterized by nearly linear oxo-ligands (O = U=O), uranium-phosphate species formed through microbial U reduction lack these distinctive double-bonded oxo-ligands (Morin et al., 2016). The U^{6+} reference material used here is a hydrated uranyl-nitrate compound. In marine environments, however, uranyl-triscarbonato species incorporate into aragonite and calcite lattices with no or little change in coordination chemistry – that is, as a distinct species with ligands differing from those of the reference material (Reeder et al., 2001; Reeder et al., 2000). These differences in local bonding environment may cause shifts in absorbance peaks and variations in spectral features between U^{4+} and U^{6+} references and U^{4+} and U^{6+} in the samples when measured on the U-L_3 edge. Additionally, if pentavalent U^{5+} is present, then that may complicate ITFA interpretations further, since U^{5+} is not resolvable as a significant shift in absorbance peak of the U-L_3 edge. A better agreement between spectroscopic and chromatographic results arises when the U^{5+}-U^{6+} oxyhydroxide $U^{5+}(H_2O)_2(U^{6+}O_2)_2O_4(OH)(H_2O)_2$ is included as a third component in the ITFA fit. In fact, applying a three-component fit dramatically decreases the estimated U^{4+} content especially in the two shallow samples. With all three reference materials included, U^{4+} accounts for 24–46 % of total U in the deeper Malo Jezero sediments from 20-40 cm depth, and declining from nearly ~ 100 % to 46–75 % in the surface sediments (Table 4). Thus, more appropriate reference materials may reduce the discrepancy between HERFD-XANES and ion chromatographic estimates of U^{4+} and U^{6+} contents.

Conclusively, we need an improved assessment of the carbonate-associated U^{4+} and U^{5+} phases in marine sedimentary environments. To move forward, we recommend more extraction experiments testing procedural oxidation (e.g. a systematic study of the effect of extraction yields, deliberate oxidation experiments with a mix of redox sensitive metals) and development of U-M_4 edge HERFD-XANES spectroscopy applicable to ppm-level samples. Using the U-M_4 edge would directly probe oxidation state through the 3d-5f spectroscopic transitions compared to the U-L_3 edge, which is easier analyzable but more coordination sensitive (Kvashnina et al., 2013; Kvashnina and Butorin, 2022).

4.2. Characterization of U in modern carbonate sediments

Importantly, we observe that U^{4+} accumulates with depth in the iron- and sulfate-reducing zones of the aragonitic and calcitic Malo Jezero sediments (Figs. 3 & 5). Further, air-exposed samples that were dried aerobically prior to analysis contain little to no U^{4+}, regardless of the sediment depth and redox zone from which they were collected. This observation indicates that the accumulating U^{4+} resides in labile, air- and oxidation-sensitive phase(s). The presence of highly oxidation-sensitive U^{4+} phases in the Malo Jezero carbonate sediments is coherent with recent evidence that microbial U reduction produces various non-crystalline and labile U^{4+} phases in other reducing environments (Alessi et al., 2014; Bhattacharyya et al., 2017; Bone et al., 2020; Cerrato et al., 2013; Morin et al., 2016).

There are likely two main authigenic sources of U to the sediments: (1) dissolved U^{6+} carbonate anions diffusing across the sediment–water interface that are reductively immobilized inside the sediments and/or perhaps directly incorporated into diagenetic minerals, and (2) particulate U^{6+} captured in primary authigenic carbonate, such as aragonite deposited onto the sediment pile during whiting events (Sondi et al., 2010). The extraction results show that the U^{4+} fraction increases from ~ 0 % to ~ 45 % and that total U_{bulk} content increases from 3.7 to 6.1 μg/g in the uppermost ~ 5 cm of the sediment column. This downwards increase in both U content and U^{4+} fraction, suggests that the downwards diffusive U flux (Fig. 5) is immobilized via reduction, and delivers a substantial fraction of the U present in the Malo Jezero sediments. Interestingly, U^{6+} still accounts for upwards of half of the HCl-extractable uranium (U_{HCl}) throughout the sediment core (Table 2).

4.3. Uranium burial and rapid redox-sensitive recycling in marine carbonate settings

The steady increase in the U^{4+}_{HCl} fraction in the uppermost 5 cm of the sediment column stands in contrast to the abrupt and large isotope offset immediately below the SWI. The most surficial sediments have $\delta^{238}U_{auth}$ values offset by 0.65 ± 0.17 ‰ relative to dissolved U in the overlying water column (Fig. 8, Bura-Nakić et al. (2020)). This isotopic offset indicates that surficial sedimentary U_{auth} (~ U_{HCl}) has experienced significant reductive isotope fractionation, despite consisting predominantly of U^{6+}. We propose a model of U delivery and syndepositional/early diagenesis in Malo Jezero that accounts for the decoupling of U oxidation states and U isotope compositions in the sediments through extensive redox-sensitive U cycling near the sediment–water interface.

The $\delta^{238}U_{auth}$ value of authigenic U in the Malo Jezero sediment cores is offset from overlying seawater immediately at the sediment–water interface by at least + 0.65 ± 0.17 ‰. Additionally, if some portion of the authigenic U is, in fact, U^{6+} hosted in primary carbonate minerals with seawater δ ^{238}U composition, then the + 0.65 ± 0.17 ‰ offset is diluted and the effective isotope fractionation expressed in the sedimentary U^{4+} must be even greater. The magnitude of the isotope offset is similar to the isotope fractionation between reactant and product for microbial U reduction (up to + 1 ‰; Basu et al., 2020). Given only 13 % of U_{HCl} was extracted as reduced U^{4+} at 0–1 cm depth, where the U isotope offset is largest, we infer that most of the microbial reduction products have been quantitatively oxidized likely near the sediment–water interface. This reoxidation might occur in a process like that observed when UO_2 and U^{5+}-magnetite is oxidized upon air exposure. The reoxidation process may occur with a 'rind effect' where one

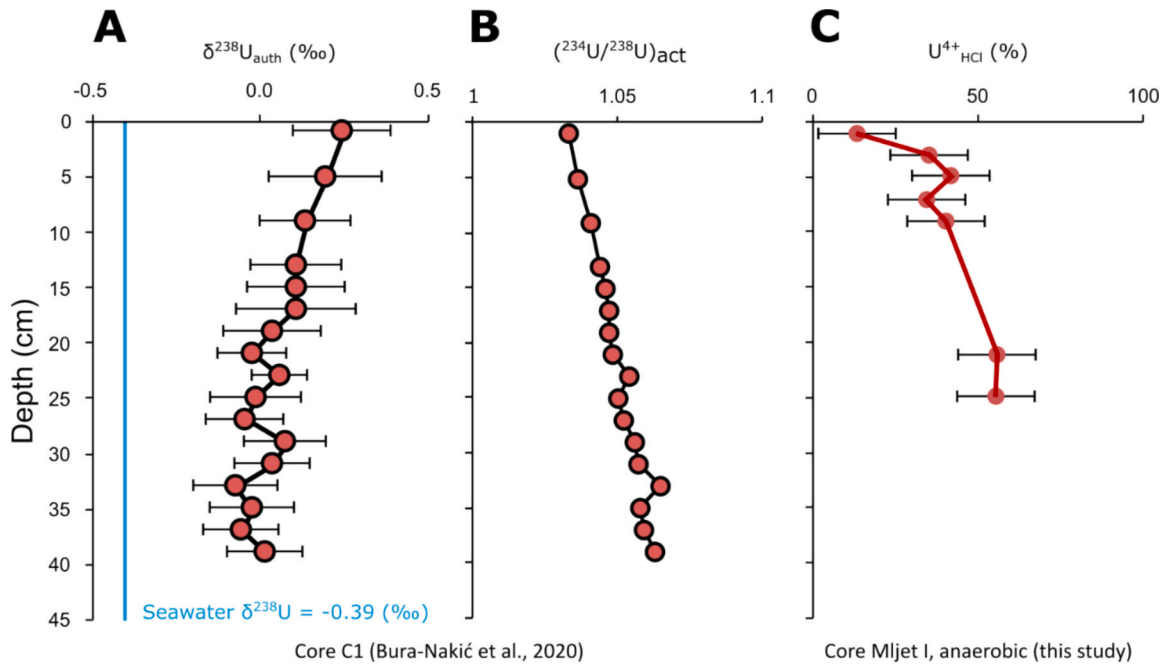

Fig. 8. $\delta^{238}U$ (A) and $(^{234}U/^{238}U)_{act}$ (B) data with 2SD error of the C1 core from Bura-Nakić et al. (2020) plotted together with downcore evolution of the U^{4+}/U_{HCl} ratio (C) of the Mljet I core (this study). 2SD of $(^{234}U/^{238}U)_{act}$ is smaller than the size of the symbols. Uncertainties given on U^{4+}/U_{HCl} ratios are the 2SE of the weighted average of repeat measurements given in Table 1.

layer of the reduced U is completely oxidized before the next layer is exposed to the oxidant. Hence, this will impart little or no U isotope fractionation and does not counter the isotope fractionation imparted by original microbial reduction (Pan et al., 2022; Wang et al., 2015).

Oxidation of U^{4+} may occur on mineral surfaces with Fe^{3+}-containing oxide minerals present in the environment (Ginder-Vogel et al., 2006; Ginder-Vogel et al., 2010; Sani et al., 2004; Sani et al., 2005; Wan et al., 2005). Biogenic non-crystalline U^{4+} is strongly susceptible to oxidation even under short periods of oxidative conditions (Cerrato et al., 2013; Newsome et al., 2015). Thus, labile U^{4+} or U^{5+} phases hosted in microbial reduction products (Vettese et al., 2020) could naturally experience periods of oxidation depending upon decomposition of cell material and fluctuations in the O_2 penetration depth (perhaps modulated by the occurrence of bioturbating animals). With sediment depth and declining redox potential, this reoxidation likely ceases, and labile U^{4+} becomes the dominant HCl-leachable U-bearing phase.

If surficial U^{6+} is indeed a product of rapid reoxidation of microbially reduced uranium, as we propose, it must be, at least temporarily, stabilized in the sediment following reoxidation. While the exact form of this U^{6+} phase remains unidentified, several possibilities exist. For instance, the uranyl-triscarbonato ion readily integrates into the aragonite lattice, suggesting that diagenetic carbonate transformations may provide host minerals for U^{6+} (Reeder et al., 2000). Hexavalent U^{6+} can also adsorb onto iron hydroxide surfaces; in oxic bicarbonate solutions with low concentrations of environmentally relevant U, 80–100 % of U^{6+} binds to hematite within the pH range of 7–8 (Ho and Miller, 1986). Additionally, hexavalent U can precipitate as insoluble compounds, including uranyl-hydroxides (such as schoepite), uranyl-phosphates (e.g., autunite), and, under conditions of high pCO_2—such as in respiration-rich waters—uranyl-carbonates (e.g., rutherfordine) (Burns and Finch, 1999). Indeed, if one assumes environmentally relevant concentrations of $Ca^{2+} = 10$ mM, $PO_4^{3-} = 0.2$ μM, $CO_3^{2+} = 0.05$ μM, and a pH of 7, then the uranyl ion is saturated with respect to metaschoepite, autunite and rutherfordine at concentrations of 2.2 nM, 0.02 nM, and 30 nM, respectively (Mühr-Ebert et al., 2019). Supporting evidence comes from analyses of calcite- and dolomite-rich, U-contaminated topsoils by Morris et al. (1996), which indicate that hexavalent U is both prevalent (constituting 75–95 % of bulk U) and stabilized in schoepite- and autunite-like phases. In any case, the destiny of U^{6+} forming on early diagenetic phases depends on its stability.

Clearly, uranium removal from pore fluids into sediments proceeds at greater depths inside the sediments. Although, we did not measure the oxidation state of U in the pore fluids, it is likely that U exists primarily as the hexavalent Ca-uranyl-triscarbonato species in Ca-rich anoxic porewater (Anderson et al., 1989; Brooks et al., 2003; Kelly et al., 2006). Residual dissolved U^{6+} from microbial reduction will have a light $\delta^{238}U$ value, complementary to the heavy $\delta^{238}U$ value of initial reduction products. With depth this downwards diffusing residual U likely precipitates by microbial reduction or perhaps via incorporation of hexavalent U into diagenetic carbonate minerals (Bura-Nakić et al., 2020). Reductive U removal in a closed-system manner can explain the gradual trend with depth towards more seawater-like $\delta^{238}U$ values (approaching –0.4 ‰), as well as more seawater-like $^{234}U/^{238}U_{act}$ ratios (approaching 1.147), as well as the increasing proportion of tetravalent uranium with depth inside the sediments (Fig. 8).

4.4. *Implications for paleo-seawater $\delta^{238}U$ reconstructions*

We have demonstrated that a range of modern carbonate mud and ancient limestone rock samples contain both U^{6+} and U^{4+} phases. The preservation of mixed U oxidation states in ancient carbonate samples opens interesting avenues to improve paleo-seawater $\delta^{238}U$ reconstructions that currently suffer from diagenetic overprints of variable, and currently unpredictable, magnitude (Chen et al., 2018; del Rey et al., 2020). Our model suggests that microbial U^{6+} reduction produces air-sensitive U phases that are easily oxidized, and that the oxidation step imposes little or no isotopic consequences on the sediment. This means that hexavalent U in sediments either carries seawater isotope composition (e.g. in primary aragonite and calcite minerals) or a heavier $\delta^{238}U$ value depending on whether carbonate sediments naturally host oxidized microbial reduction products.

So far, we have seen no indication that U^{4+} in geological rock samples is oxidized during sample treatment in the laboratory. Possibly, the

$\delta^{238}U$ value of the individual U^{4+} and U^{6+} fractions can help elucidate the extent of U cycling at the sediment–water interface, the syngenetic and diagenetic origins and perhaps help to quantify the 'openness' of the sediment system with respect to reductive U removal and exchange with the overlying water column. In this light, our anaerobic extraction method offers an interesting new avenue for oxidation-state specific U isotope analyses in carbonate materials that can help fingerprint redox-dependent U cycling in the (sub)surface environment and improve paleoredox reconstructions by identifying specific U^{6+} phases in rocks that are more likely to preserve the composition of ancient seawater.

5. Conclusions and perspective

The determination of U oxidation states in Malo Jezero carbonates in this study reveals a complex system of redox and isotopic transformations affecting uranium during syndepositional diagenesis in carbonate settings. The anaerobic extraction method developed here provides new opportunities to understand these processes in greater detail.

Our results demonstrate that the TEVA resin-based procedure for anaerobic ion-exchange separation of U^{4+} and U^{6+} is a viable method for studying U oxidation state distributions in both modern and ancient carbonate sediments. The proportion of U^{4+} in carbonate matrices can be reliably reproduced when care is taken to perform leaches anaerobically and minimize procedural oxidation. Therefore, we stress the need to monitor procedural oxidation in future extraction and recommend that synchrotron data is collected under cryo and/or strictly anoxic conditions.

We have performed HERFD-XANES analyses in marine carbonate sediments containing as little as ~ 1 ppm U, comparable to the U concentration in the average upper crust, demonstrating a new pathway for investigating bulk uranium speciation in most environmental solid samples. Yet, more environmentally relevant uranium reference materials are necessary to assess the accuracy of bulk U oxidation state analysis.

We propose a model for early diagenetic U cycling in carbonate sediments, in which U enters the sediment primarily as U^{6+} incorporated in hydrogenous aragonite, and as isotopically fractionated labile, non-crystalline, and nanometric U^{4+} that can undergo extensive re-oxidation within the upper millimeters to centimeters of the sediment. As residual oxidants become scarcer with depth inside the sediment, microbially reduced U^{4+} increases at the expense of labile U^{6+} and likely a subordinate fraction of the residual U^{6+} that escaped reduction at the sediment–water interface diffuses further into the sediments and gets reductively immobilized with depth.

Our method to separate U^{6+} and U^{4+} provides intriguing prospects for oxidation-state-specific U isotope analyses of carbonate sediments. Isotope analyses of hexavalent uranium in carbonates may offer a more reliable record of ancient seawater compositions, providing more accurate paleoredox reconstructions with less uncertainty induced by diagenetic overprint. Future studies of oxidation state-specific $^{234}U/^{238}U$ ratios in diagenetic environments may enlighten the dynamics of what U reservoirs partake in U redox cycling and constrain directions of U movement between distinct mobile and immobile phases.

CRediT authorship contribution statement

Kasper Primdahl Olesen: Writing – review & editing, Resources. **Elvira Bura-Nakic:** Writing – review & editing, Resources. **Ivan N. Pidchenko:** Writing – review & editing, Investigation. **Kristina O. Kvashnina:** Writing – review & editing, Validation, Resources. **Tais W. Dahl:** Writing – review & editing, Writing – original draft, Validation, Supervision, Resources, Project administration, Investigation, Funding acquisition, Conceptualization.

Declaration of competing interest

The authors declare that they have no known competing financial interests or personal relationships that could have appeared to influence the work reported in this paper.

Acknowledgements

With appreciation, we acknowledge S. Bruggmann, three anonymous reviewers, and the editor for their insightful and encouraging feedback, which greatly strengthened this work. We also thank Nevenka Mikac for providing sediment samples from Mljet lake 2011, I. Živković and T. Bulat (Ruđer Bošković Institute, Croatia) for assistance during sampling in 2019. S. Willatzen is thanked for his contribution to data collection, which were carried out as part of his MSc thesis work at University of Copenhagen, Denmark. We also thank J. Chen (Nanjing Institute of Palaeontology and Geological Sciences) for guidance and support during field work to collect Carboniferous carbonate samples in South China. T. Frickmann and D. E. Canfield is thanked for assistance with ICPMS analyses at University of Southern Denmark. TWD acknowledges financial support from the Carlsberg Foundation infrastructure grant (CF15-0331) and Distinguished Associate Professor program (CF16–0876), the Danish Council for Independent Research (7014-00295B and 8102-00005B). EBN acknowledges financial support from the Croatian Science Foundation (project IP-2018-01-7813, "REDOX").

Appendix A. Supplementary material

Supplementary Material contains a supplementary table 1 with raw U^{4+} and U^{6+} measurements of all individual data points, and a supplementary figure 1 U^{4+} concentrations plotted against Rb concentrations of the HCl-leached Mljet I core. Supplementary material to this article can be found online at https://doi.org/10.1016/j.gca.2025.07.006.

Data availability

All data appearing in the paper and any supplements, including spectra, are now archived in the open access repository at University of Copenhagen's Electronic Data Archive (ERDA): https://doi.org/10.17894/ucph.a78828e7-ff0d-4f19-adde-08b663e8d107

References

Alessi, D.S., et al., 2014. The product of microbial uranium reduction includes multiple species with U(IV)–phosphate coordination. Geochim. Cosmochim. Acta 131, 115–127.
Andersen, M.B., et al., 2014. A modern framework for the interpretation of 238U/235U in studies of ancient ocean redox. Earth Planet. Sci. Lett. 400, 184–194.
Andersen, M.B., Stirling, C.H., Weyer, S., 2017. Uranium Isotope Fractionation. Rev. Mineral. Geochem. 82 (1), 799–850.
Anderson, R.F., 1984. A Method for determining the Oxidation State of Uranium in Natural Waters. Nucl. Instrum. Methods Phys. Res. 223, 213–217.
Anderson, R.F., Fleisher, M.Q., LeHuray, A.P., 1989. Concentration, oxidation state, and particulate flux of uranium in the Black Sea. Geochim. Cosmochim. Acta 53, 2215–2224.
Basu, A., et al., 2020. Microbial U Isotope Fractionation Depends on the U(VI) Reduction Rate. Environ. Sci. Technol. 54 (4), 2295–2303.
Benociv, A., et al., 2000. Ecological characteristics of the Mljet Island seawater lakes (South Adriatic Sea) with special reference to their resident populations of medusae. Sci. Mar. 64, 197–206.
Berner, R.A., VandenBrooks, J.M., Ward, P.D., 2007. Oxygen and Evolution. Science 316, 557–558.
Bhattacharyya, A., et al., 2017. Biogenic non-crystalline U((IV)) revealed as major component in uranium ore deposits. Nat. Commun. 8, 15538.
Bone, S.E., et al., 2020. Complexation by Organic Matter Controls Uranium Mobility in Anoxic Sediments. Environ. Sci. Technol. 54 (3), 1493–1502.
Brooks, S.C., et al., 2003. Inhibition of bacterial U(VI) reduction by calcium. Environ. Sci. Technol. 37 (9), 1850–1858.
Brown, S.T., Basu, A., Ding, X., Christensen, J.N., DePaolo, D.J., 2018. Uranium isotope fractionation by abiotic reductive precipitation. Proc. Natl. Acad. Sci. U. S. A. 115 (35), 8688–8693.
Bura-Nakić, E., Sondi, I., Mikac, N., Andersen, M.B., 2020. Investigating the molybdenum and uranium redox proxies in a modern shallow anoxic carbonate rich marine

sediment setting of the Malo Jezero (Mljet Lakes. Adriatic Sea), Chemical Geology, p. 533.
Burns, P.C., Finch, R., 1999. Uranium: Mineralogy, Geochemistry and the Environment. Reviews in Mineralogy. Mineralogical Society of America, Washington, DC.
Canfield, D.E., 2005. THE EARLY HISTORY OF ATMOSPHERIC OXYGEN: Homage to Robert M. Garrels. Annu. Rev. Earth Planet. Sci. 33 (1), 1–36.
Canfield, D.E., Naemi, A., 2025. Dynamics of particle transport from soils to the sea. R. Soc. Open Sci. 12.
Cerrato, J.M., et al., 2013. Relative reactivity of biogenic and chemogenic uraninite and biogenic noncrystalline U(IV). Environ. Sci. Technol. 47 (17), 9756–9763.
Chen, J., et al., 2016a. Coupled sedimentary and δ13C records of late Mississippian platform-to-slope successions from South China: Insight into δ13C chemostratigraphy. Palaeogeogr. Palaeoclimatol. Palaeoecol. 448, 162–178.
Chen, X., Robinson, S.A., Romaniello, S.J., Anbar, A.D., 2022. 238U/235U in calcite is more susceptible to carbonate diagenesis. Geochim. Cosmochim. Acta 326, 273–287.
Chen, X., Romaniello, S.J., Anbar, A.D., 2017. Uranium isotope fractionation induced by aqueous speciation: Implications for U isotopes in marine CaCO 3 as a paleoredox proxy. Geochim. Cosmochim. Acta 215, 162–172.
Chen, X., et al., 2018. Diagenetic effects on uranium isotope fractionation in carbonate sediments from the Bahamas. Geochim. Cosmochim. Acta 237, 294–311.
Chen, X., Romaniello, S.J., Herrmann, A.D., Wasylenki, L.E., Anbar, A.D., 2016b. Uranium isotope fractionation during coprecipitation with aragonite and calcite. Geochim. Cosmochim. Acta 188, 189–207.
Chen, X., et al., 2021. Anoxic depositional overprinting of 238U/235U in calcite: when do carbonates tell black shale tales? Geology 49 (10), 1193–1197.
Clarkson, M.O., et al., 2021. Carbonate associated uranium isotopes as a novel local redox indicator in oxidatively disturbed reducing sediments. Geochim. Cosmochim. Acta 311, 12–28.
Clarkson, M.O., Müsing, K., Andersen, M.B., Vance, D., 2020. Examining pelagic carbonate-rich sediments as an archive for authigenic uranium and molybdenum isotopes using reductive cleaning and leaching experiments. Chem. Geol. 539.
Cole, D.B., et al., 2020. On the co-evolution of surface oxygen levels and animals. Geobiology 18 (3), 260–281.
Dahl, T.W., et al., 2014. Uranium isotopes distinguish two geochemically distinct stages during the later Cambrian SPICE event. Earth Planet. Sci. Lett. 401, 313–326.
Dahl, T.W., et al., 2017. Reorganisation of Earth's biogeochemical cycles briefly oxygenated the oceans 520 Myr ago. Geochem. Perspect. Lett. 210–220.
De Bona, E., et al., 2022. Oxidation of Micro- and Nanograined UO(2) Pellets by In Situ Synchrotron X-ray Diffraction. Inorg. Chem. 61 (4), 1843–1850.
del Rey, Á., Havsteen, J.C., Bizzarro, M., Dahl, T.W., 2020. Untangling the diagenetic history of uranium isotopes in marine carbonates: a case study tracing the δ238U composition of late Silurian oceans using calcitic brachiopod shells. Geochim. Cosmochim. Acta 287, 93–110.
Dong, W., Brooks, S.C., 2006. Determination of the Formation Constants of Ternary Complexes of Uranyl and Carbonate with Alkaline Earth Metals (Mg2+,Ca2+,Sr2+, and Ba2+) using Anion Exchange Method. Environ. Sci. Technol. 40, 4689–4695.
Du, X., et al., 2011. Reduction of uranium(VI) by soluble iron(II) conforms with thermodynamic predictions. Environ. Sci. Technol. 45 (11), 4718–4725.
Dunk, R.M., Mills, R.A., Jenkins, W.J., 2002. A reevaluation of the oceanic uranium budget for the Holocene. Chem. Geol. 190, 45–67.
Ervanne, H., 2004a. Detecting and minimizing interferences in uranium oxidation states during dissolution of solid phases. J. Radioanal. Nucl. Chem. 260 (2), 249–253.
Ervanne, H., 2004b. Oxidation state analyses of Uranium with emphasis on chemical speciation in geological media. University of Helsinki 55, pp.
Gavini, M.B., Rocco, F.G., Kim, S.M., 1987. A new radiochemical procedure for uranium assay in environmental samples. J. Radioanal. Chem. 67 (2), 437–444.
Gerber, E., et al., 2021. Insight into the structure–property relationship of UO2 nanoparticles. Inorg. Chem. Front. 8 (4), 1102–1110.
Ginder-Vogel, M., Criddle, C.S., Fendorf, S., 2006. Thermodynamic Constraints on the Oxidation of Biogenic UO2 by Fe(III) (Hydr)oxides. Environ. Sci. Technol. 40 (11), 3544–3550.
Ginder-Vogel, M., Stewart, B., Fendorf, S., 2010. Kinetic and Mechanistic Constraints on the Oxidation of Biogenic Uraninite by Ferrihydrite. Environ. Sci. Technol. 44 (1), 163–169.
Golubitskii, G.B., Budko, E.V., Basova, E.M., Kostarnoi, A.V., Ivanov, V.M., 2007. Stability of ascorbic acid in aqueous and aqueous-organic solutions for quantitative determination. J. Anal. Chem. 62 (8), 742–747.
Greene, P.M., Balfe, P.E., 1980. Stratigraphic drilling report–GSQ Mt Whelan 1 and 2.
Ho, C.H., Miller, N.H., 1986. Formation of uranium oxide sols in bicarbonate solutions. J. Colloid Interface Sci. 113 (1), 232–240.
Holland, H., 2002. Volcanic gases, black smokers, and the Great Oxidation Event. Geochim. Cosmochim. Acta 66 (21), 3811–3826.
Holland, H.D., 2006. The oxygenation of the atmosphere and oceans. Philos. Trans. R. Soc. Lond. B Biol. Sci. 361 (1470), 903–915.
Holmden, C., Amini, M., Francois, R., 2015. Uranium isotope fractionation in Saanich Inlet: a modern analog study of a paleoredox tracer. Geochim. Cosmochim. Acta 153, 202–215.
Hood, A.v.S. et al., 2016. Integrated geochemical-petrographic insights from component-selective δ238U of Cryogenian marine carbonates. Geology, 44(11): 935-938.
Horwitz, E.P., et al., 1995. Separation and preconcentration of actinides by extraction chromatography using a supported liquid anion exchanger: application to the characterization of high-level nuclear waste solutions. Anal. Chim. Acta 310, 63–78.
Hussonnois, M., Guillaumont, R., Brillard, L., Fattahi, M., 1989. A Method for determining the oxidation state of Uranium at concentrations as low as 10^-10M. Mater. Res. Soc. Symp. Proc. 127, 979–984.
Janeczek, J., Ewing, R.C., Thomas, L.E., 1993. Oxidation of uraninite: does tetragonal U3O7 occur in nature? J. Nucl. Mater. 207, 177–191.
Kelly, S.D., Kemner, K.M., Brooks, S.C., 2007. X-ray absorption spectroscopy identifies calcium-uranyl-carbonate complexes at environmental concentrations. Geochim. Cosmochim. Acta 71 (4), 821–834.
Kelly, S.D., et al., 2003. Uranyl incorporation in natural calcite. Environ. Sci. Technol. 37, 1284–1287.
Kelly, S.D., Rasbury, E.T., Chattopadhyay, S., Kropf, A.J., Kemner, K.M., 2006. Evidence of a Stable Uranyl Site in Ancient Organic- Rich Calcite. Environ. Sci. Technol. 40 (7), 2262–2268.
Korkisch, J., Farag, A., Hecht, F., 1958. Eine neue Methode zur Bestimmung des Urans in Phosphaten, Kohlenaschen, Bauxiten usw. mittels Ionenaustausches. Fresenius' Zeitschrift Für Analytische Chemie 161, 92–100.
Kosog, B., La Pierre, H.S., Denecke, M.A., Heinemann, F.W., Meyer, K., 2012. Oxidation state delineation via U L(III)-edge XANES in a series of isostructural uranium coordination complexes. Inorg. Chem. 51 (14), 7940–7944.
Kvashnina, K.O., Kvashnin, Y.O., Butorin, S.M., 2014. Role of resonant inelastic X-ray scattering in high-resolution core-level spectroscopy of actinide materials. J. Electron Spectrosc. Relat. Phenom. 194, 27–36.
Kvashnina, K.O., Scheinost, A.C., 2016. A Johann-type X-ray emission spectrometer at the Rossendorf beamline. J. Synchrotron Radiat. 23 (Pt 3), 836–841.
Langmuir, D., 1978. Uranium solution-mineral equilibria at low temperatures with applications to sedimentary ore deposits. Geochim. Cosmochim. Acta 42, 547–569.
Le Pape, P., et al., 2020. HERFD-XANES spectroscopy at the U M-edge applied to the analysis of U oxidation state in a heavily contaminated wetland soil. Appl. Geochem. 122.
Lenton, T.M., Boyle, R.A., Poulton, S.W., Shields-Zhou, G.A., Butterfield, N.J., 2014. Co-evolution of eukaryotes and ocean oxygenation in the Neoproterozoic era. Nat. Geosci. 7 (4), 257–265.
Livermore, B.D., Dahl, T.W., Bizzarro, M., Connelly, J.N., 2020. Uranium isotope compositions of biogenic carbonates – Implications for U uptake in shells and the application of the paleo-ocean oxygenation proxy. Geochim. Cosmochim. Acta 287, 50–64.
Lojen, S., Sondi, I., Juracic, M., 2010. Geochemical conditions for the preservation of recent aragonite-rich sediments in Mediterranean karstic marine lakes (Mljet Island, Adriatic Sea, Croatia). Mar. Freshw. Res. 61 (1).
Lyons, T.W., Reinhard, C.T., Planavsky, N.J., 2014. The rise of oxygen in Earth's early ocean and atmosphere. Nature 506 (7488), 307–315.
Malinowski, E.R., 1977. Determination of the number of factors and the experimental error in a data matrix. Anal. Chem. 49 (4), 612–617.
Morin, G., et al., 2016. Mononuclear U(IV) complexes and ningyoite as major uranium species in lake sediments. Geochem. Perspect. Lett.
Morris, D.E., et al., 1996. Speciation of Uranium in Fernald Soils by Molecular Spectroscopic Methods: Characterization of Untreated Soils. Environ. Sci. Technol. 30 (7), 2322–2331.
Morse, J.W., Mackenzie, F.T., 1990. Geochemistry of Sedimentary Carbonates. Elsevier, New York.
Mühr-Ebert, E.L., Wagner, F., Walther, C., 2019. Speciation of uranium: Compilation of a thermodynamic database and its experimental evaluation using different analytical techniques. Appl. Geochem. 100, 213–222.
Newsome, L., Morris, K., Shaw, S., Trivedi, D., Lloyd, J.R., 2015. The stability of microbially reduced U(IV); impact of residual electron donor and sediment ageing. Chem. Geol. 409, 125–135.
Noordmann, J., et al., 2015. Uranium and molybdenum isotope systematics in modern euxinic basins: Case studies from the central Baltic Sea and the Kyllaren fjord (Norway). Chem. Geol. 396, 182–195.
Pan, Z., et al., 2022. Persistence of the Isotopic Signature of Pentavalent Uranium in Magnetite. Environ. Sci. Technol. 56 (3), 1753–1762.
Pidchenko, I., Salminen-Paatero, S., Rothe, J., Suksi, J., 2013. Study of uranium oxidation states in geological material. J. Environ. Radioact. 124, 141–146.
Pingitore, N.E., Iglesias, A., Lytle, F., Wellington, G.M., 2002. X-Ray absorption spectroscopy of uranium at low ppm levels in coral skeletal aragonite. Microchem. J. 71, 261–266.
Prieur, D., et al., 2025. Frontiers of Synchrotron Methods for Actinide Science. Chemistry-Methods.
Rademacher, L.K., et al., 2006. Experimentally determined Uranium isotope fractionation during reduction of hexavalent U by bacteria and zero valent Iron. Environ. Sci. Technol. 40, 6943–6948.
Răileanu, M., Cecal, A., 2008. Separation of U(IV) and U(VI) species by means of ion-exchange resins of the DGA-, TEVA- and UTEVA-type. J. Radioanal. Nucl. Chem. 277 (3), 587–590.
Rasbury, E.T., et al., 2021. Tools for uranium characterization in carbonate samples: case studies of natural U–Pb geochronology reference materials. Geochronology 3 (1), 103–122.
Reeder, R.J., et al., 2001. Coprecipitation of Uranium(VI) with Calcite: XAFS, micro-XAS, and luminescence characterization. Geochim. Cosmochim. Acta 65 (20), 3491–3503.
Reeder, R.J., Nugentm, M., Lamble, G.M., Tait, C.D., Morris, D.E., 2000. Uranyl Incorporation into Calcite and Aragonite: XAFS and Luminescence Studies. Environ. Sci. Technol. 34, 638–644.
Reinhard, C.T., Planavsky, N.J., Olson, S.L., Lyons, T.W., Erwin, D.H., 2016. Earth's oxygen cycle and the evolution of animal life. Proc. Natl. Acad. Sci. 113 (32), 8933–8938.
Roebbert, Y., et al., 2021. Uranium Isotope Fractionation during the Anoxic Mobilization of Noncrystalline U(IV) by Ligand Complexation. Environ. Sci. Technol. 55 (12), 7959–7969.

Rolison, J.M., Stirling, C.H., Middag, R., Rijkenberg, M.J.A., 2017. Uranium stable isotope fractionation in the Black Sea: Modern calibration of the 238U/235U paleo-redox proxy. Geochim. Cosmochim. Acta 203, 69–88.
Romaniello, S.J., Herrmann, A.D., Anbar, A.D., 2013. Uranium concentrations and 238U/235U isotope ratios in modern carbonates from the Bahamas: Assessing a novel paleoredox proxy. Chem. Geol. 362, 305–316.
Rossberg, A., Reich, T., Bernhard, G., 2003. Complexation of uranium(VI) with protocatechuic acid-application of iterative transformation factor analysis to EXAFS spectroscopy. Anal. Bioanal. Chem. 376 (5), 631–638.
Rossberg, A., et al., 2009. Identification of Uranyl Surface Complexes on Ferrihydrite: Advanced EXAFS Data Analysis and CD-MUSIC Modeling. Environ. Sci. Technol. 43 (5), 1400–1406.
Saito, N., 1984. Selected data on ion exchange separations in radioanalytical chemistry. Pure Appl. Chem. 56 (4), 523–539.
Sani, R.K., Peyton, B.M., Amonette, J.E., Geesey, G.G., 2004. Reduction of uranium(VI) under sulfate-reducing conditions in the presence of Fe(III)-(hydr)oxides. Geochim. Cosmochim. Acta 68 (12), 2639–2648.
Sani, R.K., Peyton, B.M., Dohnalkova, A., Amonette, J.E., 2005. Reoxidation of Reduced Uranium with Iron(III) (Hydr)Oxides under Sulfate-reducing Conditions. Environ. Sci. Technol. 39 (7), 2059–2066.
Scheinost, A.C., et al., 2021. ROBL-II at ESRF: a synchrotron toolbox for actinide research. J. Synchrotron Radiat. 28 (Pt 1), 333–349.
Sondi, I., Juračić, M., 2010. Whiting events and the formation of aragonite in Mediterranean Karstic Marine Lakes: new evidence on its biologically induced inorganic origin. Sedimentology 57 (1), 85–95.
Sondi, I., et al., 2017. Geochemistry of recent aragonite-rich sediments in Mediterranean karstic marine lakes: Trace elements as pollution and palaeoredox proxies and indicators of authigenic mineral formation. Chemosphere 168, 786–797.
Stetten, L., et al., 2018. Redox Fluctuations and Organic Complexation govern Uranium Redistribution from U(IV)-Phosphate Minerals in a Mining-Polluted Wetland Soil, Brittany. France. Environ Sci Technol 52 (22), 13099–13109.
Stirling, C.H., Andersen, M.B., Potter, E.-K., Halliday, A.N., 2007. Low-temperature isotopic fractionation of uranium. Earth Planet. Sci. Lett. 264 (1–2), 208–225.
Stoliker, D.L., Kaviani, N., Kent, D.B., Davis, J.A., 2013. Evaluating ion exchange resin efficiency and oxidative capacity for the separation of uranium (IV) and uranium (VI). Geochem. Trans. 14 (1).
Sturchio, N.C., Antonio, M.R., Soderholm, L., Sutton, S.R., Brannon, J.C., 1998. Tetravalent uranium in calcite. Science 281 (5379), 971–973.
Stylo, M., et al., 2015. Uranium isotopes fingerprint biotic reduction. Proc. Natl. Acad. Sci. U. S. A. 112 (18), 5619–5624.
Tissot, F.L.H., et al., 2018. Controls of eustasy and diagenesis on the 238U/235U of carbonates and evolution of the seawater (234U/238U) during the last 1.4 Myr. Geochim. Cosmochim. Acta 242, 233–265.
Tissot, F.L.H., Dauphas, N., 2015. Uranium isotopic compositions of the crust and ocean: Age corrections, U budget and global extent of modern anoxia. Geochim. Cosmochim. Acta 167, 113–143.
Vettese, G.F., et al., 2020. Multiple Lines of evidence Identify U(V) as a Key Intermediate during U(VI) Reduction by Shewanella oneidensis MR1. Environ. Sci. Technol. 54 (4), 2268–2276.
Wall, J.D., Krumholz, L.R., 2006. Uranium Reduction. Annu. Rev. Microbiol. 60, 149–166.
Wan, J., et al., 2005. Reoxidation of bioreduced U under reducing conditions. Environ. Sci. Technol. 39 (16), 6162–6169.
Wang, W.-Q., et al., 2022. Constraining marine anoxia under the extremely oxygenated Permian atmosphere using uranium isotopes in calcitic brachiopods and marine carbonates. Earth Planet. Sci. Lett. 594.
Wang, X., Johnson, T.M., Lundstrom, C.C., 2015. Isotope fractionation during oxidation of tetravalent uranium by dissolved oxygen. Geochim. Cosmochim. Acta 150, 160–170.
Weyer, S., et al., 2008. Natural fractionation of 238U/235U. Geochim. Cosmochim. Acta 72 (2), 345–359.
Yuan, Y., et al., 2023. Substantial incorporation of isotopically heavy reduced U species into marine carbonate sediments. Geochim. Cosmochim. Acta 358, 27–37.
Zhang, F., et al., 2020. Uranium isotopes in marine carbonates as a global ocean paleoredox proxy: a critical review. Geochim. Cosmochim. Acta 287, 27–49.
Živković, I., Bura-Nakić, E., Knežević, L., Helz, G.R., 2023. Deposition of Mo, Re and U under contrasting redox conditions; assessment of the [Re/Mo]sw redox proxy. Geochim. Cosmochim. Acta.